

CHALMERS



High Pressure and Temperature Conversion of Lignin and Black Liquor to Liquid Fuels

*Master's Thesis within the Innovative and Sustainable Chemical Engineering
programme*

THERESE HEDLUND

Department of Energy and Environment
Division of Heat and Power Technology
CHALMERS UNIVERSITY OF TECHNOLOGY
Göteborg, Sweden 2010

MASTER'S THESIS

High Pressure and Temperature
Conversion of Lignin and Black Liquor
to Liquid Fuels

Master's Thesis within the *Innovative and Sustainable Chemical Engineering*
programme

THERESE HEDLUND

SUPERVISORS

Lars Olausson, Metso Power AB

Sven-Ingvar Andersson, Chalmers University of Technology

EXAMINER

Lennart Vamling, Chalmers University of Technology

Department of Energy and Environment
Division of Heat and Power Technology
CHALMERS UNIVERSITY OF TECHNOLOGY
Göteborg, Sweden 2010

High Pressure and Temperature Conversion of Lignin and Black Liquor to Liquid Fuels

Master's Thesis within the *Innovative and Sustainable Chemical Engineering* programme

THERESE HEDLUND

© THERESE HEDLUND 2010

Department of Energy and Environment
Division of Heat and Power Technology
Chalmers University of Technology
SE-412 96 Göteborg
Sweden
Telephone: + 46 (0)31-772 1000

Cover:

The pilot scale reactor plant used for the experimental work in this master's thesis.

Chalmers Reproservice
Göteborg, Sweden 2010

High Pressure and Temperature Conversion of Lignin and Black Liquor to Liquid Fuels

Master's Thesis within the *Innovative and Sustainable Chemical Engineering* programme

THERESE HEDLUND

Department of Energy and Environment

Division of Heat and Power Technology

Chalmers University of Technology

Abstract

A project aiming to find a method for conversion of lignin or black liquor to liquid fuels has been initiated. The conversion is supposed to take place in a high pressure and temperature reactor at near supercritical water conditions. A pilot scale autoclave station, acquired for this purpose, has been evaluated considering the heat transfer in three different units; the storage tank, the preheater and the reactor. Experiments with water have been carried out at different pressures and temperatures near the supercritical region. The temperatures of the heaters and the corresponding heated units have been measured and the results have been evaluated with mathematical models for the heat transfer. Heat transfer coefficients have been calculated both theoretically and experimentally. A difference between the theoretical and experimental overall heat transfer coefficient was found for the preheater. This difference has been investigated and the most likely cause is a small passage of air in the preheater which reduces the heat transfer from the preheater material to the water pipe. The water experiments showed that the heaters can supply enough heat to reach water temperatures near the supercritical point. Pump trials with lignin slurry at different lignin concentrations have been conducted. Slurries at higher concentrations than 10 wt% lignin could not be pumped easily with the current pump components. At these higher concentrations, the pump valves were contaminated and the flow interrupted. The results will be used in further research within the project for obtaining liquid fuels from lignin or black liquor.

Keywords: Lignin, black liquor, liquid fuel, supercritical water, autoclave, heat transfer coefficient.

Acknowledgements

I would like to thank everyone who have helped and supported me during my work on this master's thesis.

Great thanks to my supervisors; Lars Olausson and Sven-Ingvar Andersson, who have guided me through the experiments and the analysis of the results. Thanks also to Lennart Vamling for being my examiner.

I would also like to thank Bengt Erichsen for all his help with the laboratory equipment and Mathias Gourdon for helping me with the pump.

Thanks to everyone at VoM for my time in the department and especially to Erika Axén for her support during this work.

I also want to thank Metso Power AB for giving me the opportunity to do this master's thesis.

Finally, I would like to thank my family and my boyfriend for supporting me.

Table of Contents

Abstract.....	I
Acknowledgements	III
Table of Contents	V
List of Tables.....	VII
List of Figures.....	IX
Preface	XI
Notations.....	XIII
1 Introduction.....	1
1.1 Background.....	1
1.2 State of Art.....	2
1.2.1 The LignoBoost Process.....	3
1.2.2 Gasification of Lignin.....	4
1.2.3 Pyrolysis of Lignin	4
1.2.4 Hydrocracking of Lignin	5
1.2.5 Black Liquor Gasification	6
1.2.6 Pyrolysis of Black Liquor.....	7
1.2.7 Hydrogenation of Black Liquor.....	8
1.2.8 Catalytic Hydrotreating of Black Liquor Oils	9
1.2.9 Remarks.....	9
1.3 Objective.....	10
1.4 Outline of the Thesis	10
2 Experimental Methodology.....	13
2.1 Supercritical Water	13
2.1.1 Near Supercritical Water	14
2.2 Experimental Setup.....	14
2.2.1 Safety Measures.....	17
2.3 Operation of the Plant	17
2.3.1 Start Up.....	18
2.3.2 Shut Down.....	18
2.4 Experiments with Water	19

2.4.1	Thermodynamic Study of the Storage Tank.....	19
2.4.2	Thermodynamic Study of the Preheater	19
2.4.3	Thermodynamic Study of the Reactor.....	21
2.5	Experiments with Lignin	22
2.5.1	Pump Trials with Lignin Slurry.....	22
3	Results.....	23
3.1	Experiments with Water	23
3.1.1	Thermodynamic Study of the Storage Tank.....	23
3.1.2	Thermodynamic Study of the Preheater	24
3.1.3	Thermodynamic Study of the Reactor.....	27
3.2	Experiments with Lignin	28
3.2.1	Pump Trials with Lignin Slurry.....	29
4	Analysis of the Results.....	31
4.1	Mathematical Modelling.....	31
4.1.1	The Storage Tank	31
4.1.2	The Preheater.....	39
4.1.3	The Reactor	46
4.2	Control and Regulation.....	53
4.2.1	PID-regulators	53
4.2.2	Observations from Experiments.....	55
5	Discussion.....	57
5.1	Experimental Results	57
5.2	Mathematical Modelling.....	58
5.3	Accuracy of Measurements.....	60
5.4	Control and Regulation.....	61
6	Conclusions.....	63
7	Further Research	65
	References	67
	Appendix A – Storage Tank Calculations	71
	Appendix B – Preheater Calculations.....	72
	Appendix C – Reactor Calculations	75

List of Tables

Table 2.1. The different temperatures which were set for the electrical heating jacket during the storage tank experiments.....	19
Table 2.2. Experimental design for the preheater experiments. Different temperatures, mass flows and pressures were examined.	20
Table 2.3. Additional experiments for the thermodynamic study of the preheater.	20
Table 2.4. Set values of mass flow and temperatures for all reactor experiments. The experiments were carried out at a pressure of 200 bar.	21
Table 2.5. Concentration of lignin in the pump trials.....	22
Table 3.1. Output signal and the corresponding effect of the heating jacket for the different storage tank experiments.	24
Table 3.2. All results from the experiments with the preheater. The pressure could not be regulated at pressures below 200 bar for a flow rate of 3 kg/h. Thereby, there are no data for 150 and 175 bar for the highest flow rate.....	25
Table 3.3. All results from the reactor experiments. The wall temperature and the temperature of the heating jacket were measured and the output signal to the heating jacket was noted for different temperatures in and out of the reactor.	27
Table 4.1. Values of parameters used for calculation of the heat transfer coefficient of the water inside of the storage tank.	34
Table 4.2. Thickness and thermal conductivity of the tank wall.....	35
Table 4.3. Values of the parameters used for calculation of the heat transfer coefficient of the heating jacket.....	36
Table 4.4. Dimensions of the storage tank and the calculated heat exchanger area.....	37
Table 4.5. The cross sectional area and ambient temperature used for calculation of the overall heat transfer coefficient to the surroundings.	38
Table 4.6. The outside diameter and area of the heating jacket.	38
Table 4.7. The dimensions of the water pipes in the preheater and the heat exchanger area.	41
Table 4.8. The mean value of the experimentally calculated overall heat transfer coefficient for each mass flow.....	41
Table 4.9. Values of the parameters used for calculation of the heat transfer resistances in the aluminum and the pipe wall and the calculated resistances.	44
Table 4.10. The value for the thermal conductivity of magnesium oxide and the estimated diameter of the stainless steel core of the cartridge heater.....	45
Table 4.11. Dimensions and heat exchanger area for the heating jacket.....	49
Table 4.12. The diameter and area of the cylinder situated on top of the reactor.	49
Table 4.13. Parameters used for the cooling water calculations.	50
Table 4.14. Reactor dimensions and parameters for calculation of radiant heat transfer.	52
Table 4.15. Parameters for calculation of heat transport through the reactor wall.....	53
Table 4.16. Regulator parameters for the heaters of the different heated units.....	55

Table A. 1. Data and resulting values for the calculation of the heat transfer coefficient for the water in the tank. The constants C, a and b are found in the literature [25 p. 959].	71
Table A. 2. Constants used for the calculation of the heat transfer coefficient for the water in the tank. The properties of the water are found in the literature [26]. Mean values between 20 and 75°C at atmospheric pressure has been used.....	71
Table A. 3. Data and resulting values for the water heat transfer coefficient. The values for the water properties are found in the literature [32]. Mean values between 40°C and the water outlet temperature has been used at 200 bar. The mean value for the water heat transfer coefficient can be found below the table.	72
Table A. 4. Constants used for the calculation of the water heat transfer coefficient....	72
Table A. 5. Data and resulting values for the cartridge heater heat transfer from the preheater experiments.....	73
Table A. 6. Constants used for the calculation of the cartridge heater heat transfer.....	74
Table A. 7. Data and resulting values for the reactor heating. The mean value for the emissivity can be found below the table with the calculated values.	75
Table A. 8. Constants used for the reactor heating. The thermal conductivity [29], emissivity [28 p. Ka3] and Stefan-Boltzman coefficient [27 p. 209] are found in the literature.....	75

List of Figures

Figure 1.1. The energy use for different sectors in Sweden 2008 divided by energy source. The numbers are shown in TWh. [7]	2
Figure 2.1. Phase diagram of a typical fluid. The different phases are separated by the solid lines. The supercritical region is located above the critical point.....	13
Figure 2.2. The control unit.....	15
Figure 2.3. The educt box. The storage tank and the pump are the main components of the unit.	15
Figure 2.4. Process flow diagram of the reactor plant.....	16
Figure 2.5. The reactor module. The left picture shows the outside with the aluminum door and safety glass pane. The picture to the right shows the interior of the module with the preheater (a), the reactor (b), the cooler (c) and the pressure control valve (d).	17
Figure 2.6. The interior of the preheater. The cartridge heater is situated in one of the tubes in the middle, the other one is a preparation for use of two cartridge heaters. The water pipe enters and leaves the aluminum to the left in the picture.....	19
Figure 2.7. The reactor with and without the electrical heating jacket on.	21
Figure 2.8. Mixing of the lignin slurry.	22
Figure 3.1. The temperature of the water inside of the storage tank plotted against the time from start for each set temperature of the heating jacket.	23
Figure 3.2. The final temperature of the water in the storage tank for all experiments.	24
Figure 3.3. The temperatures of the aluminum and cartridge heater needed for different flow rates to obtain a temperature of the exiting water of 250°C, 280°C and 310°C respectively. All data is taken from experiments performed at 200 bar. The dashed lines represent the aluminum temperature and the continuous lines represent the temperature of the cartridge heater.	26
Figure 3.4. The results from the reactor experiments. The dashed and continuous lines represent the temperature on the outside of the reactor wall and of the heating jacket respectively. The water inlet temperature and reactor temperature are shown within brackets.....	28
Figure 4.1. Sketch of the preheating tank with heat flows and temperatures marked on the drawing.	32
Figure 4.2. The temperature profile over the heating jacket and the tank wall. The heating jacket is indicated with light grey color and the tank wall with darker grey.....	33
Figure 4.3. Cross section of the preheater. The dark grey section represents the cartridge heater, the light grey section the aluminum and the white section the water pipe. The heat flows and the temperatures are indicated in the picture.....	39
Figure 4.4. The temperature profile for the preheater. The temperature differences used to calculate the logarithmic mean temperature are also indicated in the figure.	40
Figure 4.5. Sketch over the preheater where the dimensions of the cartridge heater are marked. It can also be seen how the water pipe is wired around the cartridge heater....	44

Figure 4.6. Sketch over the reactor. The flows in and out of the reactor are indicated as well as the temperatures and heat flows.	46
Figure 4.7. The dimensions of the heating jacket.	48
Figure 4.8. Sketch of the reactor. There is a cylinder at the top of the reactor where the cooling water (cw) inlet and outlet for the stirrer are located. The cross section of this cylinder represents the heat exchange area of the top of the reactor.	49
Figure 4.9. The dimensions of the reactor.	52
Figure 4.10. Block diagram over a typical regulated system.	53
Figure 5.1. Temperature profiles. The picture to the left shows a temperature profile where the entire heat exchange area is used. The temperature increases throughout the pipe length. The right picture shows a temperature profile over a heat exchanger with an unused heat exchange area. The temperature increases a lot in the first part of the pipe, while it is kept constant through the rest of the pipe length.	59

Preface

In this master's thesis work, experiments with a pilot scale reactor have been carried out in order to investigate the heat dynamics of the reactor. Both water and lignin have been used in the experiments. The tests have been carried out from February 2010 to May 2010. The work is a first step in a research project considering conversion of lignin or alternatively black liquor to liquid fuels.

The project is carried out at the Department of Energy and Environment, Division of Heat and Power Technology, Chalmers University of Technology in cooperation with Metso Power AB.

This part of the project has been performed by Therese Hedlund with Lars Olausson and Sven-Ingvar Andersson as supervisors. All experiments have been carried out in the laboratory of the Division of Heat and Power Technology at Chalmers University of Technology.

Göteborg June 2010

Therese Hedlund

Notations

Latin letters

A	Area [m ²]
C	Circumference [m]
C_p	Heat capacity [J/kgK]
D	Diameter [m]
E	Energy [J]
e	Error signal [–]
H	Enthalpy [J/kg]
H	Height [m]
h	Heat transfer coefficient [W/m ² K]
K	Gain [–]
k	Thermal conductivity [W/mK]
L	Length [m]
\dot{m}	Mass flow [kg/s]
N	Agitator speed [rps]
P	Effect [W]
Q	Energy transfer per time unit [W]
R	Thermal resistance [m ² K/W]
T	Temperature [K] or [°C]
t	Time [s]
U	Overall heat transfer coefficient [W/m ² K]
u	Velocity [m/s]
V	Volume [m ³]
\dot{V}	Volumetric flow [m ³ /s]
y	Output signal [%]

Greek letters

ΔT	Difference in temperature [K] or [°C]
δ	Distance [m]
ϵ	Emissivity [-]
μ	Dynamic viscosity [Pas]
ρ	Density [kg/m ³]
σ	Stefan-Boltzman constant [W/m ² K ⁴]
τ	Time constant [s]

Dimensionless numbers

Nu	Nusselt number
Pr	Prandtl number
Re	Reynolds number

Indexes

Al	Aluminum
amb	Ambient
CH	Cartridge heater
cs	Cross sectional
cw	Cooling water
D	Derivative
$expr$	Experimental
H	Heating
HJ	Heating jacket
HX	Heat exchange
I	Integration
Inc	Inconel 600

<i>i</i>	Inside
<i>in</i>	Inlet
<i>L</i>	Losses
<i>lm</i>	Logarithmic mean
<i>max</i>	Maximum
<i>MgO</i>	Magnesium oxide
<i>o</i>	Outside
<i>out</i>	Outlet
<i>P</i>	Proportional
<i>PH</i>	Preheater
<i>R</i>	Reactor
<i>rad</i>	Radiant
<i>ss</i>	Stainless steel
<i>theory</i>	Theoretical
<i>top</i>	Top of the reactor
<i>tot</i>	Total
<i>w</i>	Water
<i>wall</i>	Tank/reactor wall

1 Introduction

This chapter intends to give an introduction to the master's thesis. First, the background of the subject is presented. Then a literature study of previous research within the area of conversion of lignin and black liquor to biofuel. Finally, the purpose of the work and outline of the thesis is found in this chapter.

1.1 Background

The climate change caused by increased greenhouse gas emissions has become a frequently discussed topic all over the world. The main problem is the large consumption of fossil fuels and the resulting emissions of carbon dioxide. Currently, about 80 to 85% of the accumulated carbon dioxide in the atmosphere is due to the use of fossil fuels. The other main cause is changes in land use, mainly deforestation. [1] Focus has more and more turned to replacing fossil fuels with renewable ones in order to decrease the net emissions of greenhouse gases. Fuels produced by renewable resources can be considered carbon dioxide neutral since the consumption during the photosynthesis process equals the emission during combustion. In order to achieve this shift to renewable resources, new technology and large scale processes for production are needed.

Forests have been used for many purposes, such as pulp and paper production, for a long time. The pulping waste, in form of black liquor, consists of about 60% organic compounds (mostly lignin) and about 40% recyclable pulping chemicals [2]. After being extracted from the pulp, the black liquor is evaporated to reduce the moisture content and then brought to the recovery boiler. There, the organic compound is incinerated while the pulping chemicals are recovered and brought back to the process. At the same time, steam is produced from the combustion heat. [3] The resulting steam can be used in the evaporation process and for district heating. Due to energy savings in the pulp production, more energy can be produced in the recovery boiler than what is needed in the process. [4] The excess of energy in the black liquor can thus be used for other purposes.

The lignin content can e.g. be extracted from the black liquor and processed to a solid biofuel with a high energy density and low ash content. One possible use of the solid lignin is to incinerate it in power boilers. One advantage with separation of lignin from black liquor is that it can be used to avoid an expansion of the recovery boiler if the pulp production is increased. It reduces the load of the recovery boiler, while at the same time, fuel is produced which can be used elsewhere. [5]

Black liquor gasification could be used as a replacement for the recovery boiler. The gasification combined with a steam turbine CHP (combined heat and power) unit has a higher power-to-heat ratio than combustion in a recovery boiler. [4] However, the pulping chemicals in the black liquor must still be recycled and returned to the process in order to complete the chemical cycle in the pulping plant.

Lignin and black liquor also have a potential to be used for more profitable products than heat and power. For instance, it can be used as feedstock for chemical products [6] or production of motor fuels. The transport sector is the greatest consumer of fossil fuels in Sweden. About 92%¹ of the energy used for transports in Sweden came from fossil resources in 2008 [7], which can be seen in Figure 1.1.

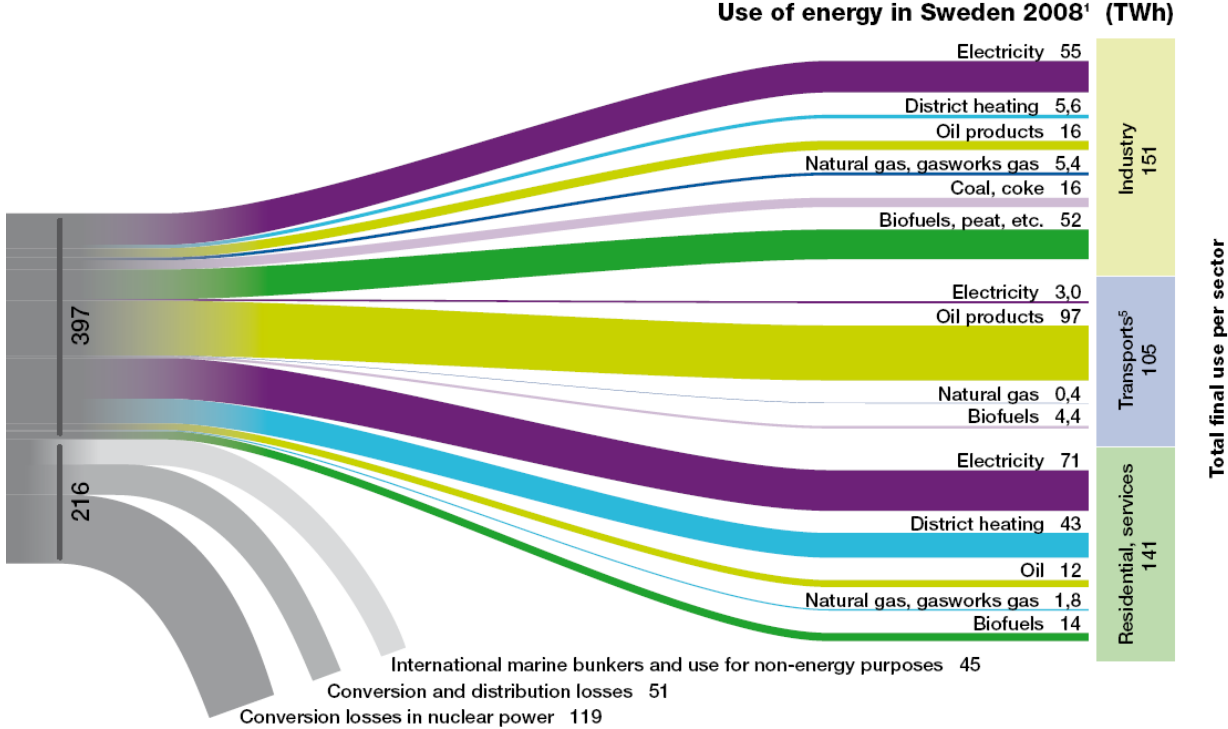


Figure 1.1. The energy use for different sectors in Sweden 2008 divided by energy source². The numbers are shown in TWh. [7]

The change from fossil fuels to fuels from renewable resources is essential to achieve a sustainable society, especially in the transport sector. Therefore, research within this area is of great importance.

1.2 State of Art

Research within the area of producing fuels from renewable resources is an important topic. New technologies need to be developed in order to increase the efficiency of the production. To achieve a global change from fossil to renewable fuels, technology has to be developed to a stage where it is economically profitable to produce biofuels.

The most emphasized concern today is to reduce the amount of carbon dioxide emissions by implementing fuels from renewable resources. However, there are other aspects that need to be considered when new techniques are developed. For instance, the use of raw material must not compromise other important functions of land use, such as food production.

¹ The number is calculated from data in [7].
² The picture is used with permission from Sweden Energy Agency.

There are many different research areas concerning new technology for production of renewable fuels. This section will discuss some of the research within conversion of lignin and black liquor to biofuel.

1.2.1 The LignoBoost Process

A technique for extraction of kraft lignin from black liquor called LignoBoost has been developed. The final product can e.g. be used as fuel in power boilers. In the extraction process, black liquor is brought from the evaporation plant to the LignoBoost plant. An acid, preferably CO₂, is added to the black liquor stream and the lignin is precipitated. The lignin is then filtered and the filtrate is recycled back to the black liquor evaporation. The filter cake, consisting of lignin, is re-dispersed and acidified again, resulting in a slurry. This slurry is filtered once more and the filtrate is also brought back to the evaporation plant. However, some part of the filtrate is used for the re-dispersion of the filter cake from the first filtration. The filter cake is finally washed with the use of displacement washing. The post-treatment of the produced filter cake is e.g. drying and pulverization. This is especially important before incineration in lime kiln burners. Furthermore, the lignin can be used for manufacturing of bio-pellets, consisting of either pure lignin or a mixture with e.g. sawdust. There are some consequences to consider when choosing the appropriate drying sequence. If small particles are created before drying, the heat and moisture transport is enhanced, but it also results in an increased risk of a dust explosion. One way of diminishing this risk is to lower the oxygen content in the heating medium. By creating larger particles, the process is safer, but not as efficient. [8]

A demonstration plant using the LignoBoost technique has been built in Bäckhammar, Sweden. It produces a solid biofuel, consisting of lignin, with high energy density and low ash content. Pilot-scale trials with incineration of extracted lignin have been carried out as a preparation for full-scale tests. The pilot trials were carried out in a powder burner at the Energy Technology Center (ETC) in Piteå, Sweden, and in a CFB (circulating fluidized bed) boiler at Chalmers University of technology in Göteborg, Sweden. In the powder burner, dried lignin powder with a particle size below 1 mm was used. Some of the conclusions from the trial were that it is possible to obtain a stable, continuous combustion of lignin and that the moisture content needs to be less than 10% for a smooth feeding of the lignin powder. During the trial with the CFB boiler, a mixture of broken lignin filter cakes and bark (15% and 85% respectively) was used as fuel. It was concluded that lignin could be co-fired with bark without disturbances in the combustion due to the fact that the filter cakes were broken into small pieces. The performance of the combustion was not affected by the lignin. Due to the sulfur content in the lignin, the alkali chloride content in the deposits was reduced. Consequently, the risk of sticky deposits and high temperature corrosion was diminished. The sulfur emission during the co-firing was higher compared to combustion with pure bark. However, most of the sulfur was captured by the calcium in the bark ash. The sintering properties of the bed material were not affected by the lignin content in the fuel. [5]

1.2.2 Gasification of Lignin

Noncatalytic gasification of lignin in supercritical water³ has been studied by Resende et al. [9]. Quartz capillary tubes with a volume of 0.58 cm³ was used as miniature batch reactors. Before the lignin was placed in the reactor, deionized water was inserted to improve mixing during heating due to its expansion. The reactor was inserted into a preheated fluidized sand bath or a tube furnace, which initiated the supercritical water gasification (SCWG). The reaction time was 2.5 – 75 minutes and the heat up time for the reactor about 30 seconds. Thereby, part of the experiments was performed at nonisothermal conditions. A base case at 600°C, 9.0 wt% biomass and a water density of 0.08 g/cm³ was chosen. These parameters were varied to investigate their influence on the gasification. It was concluded that SCWG with no catalyst present can produce gas with high yield, which contains up to 56% of the energy from the original lignin. CH₄ and CO₂ were the two main components in the resulting gas, but CO and H₂ were also produced. When no water was added to the reactor, CO was one of the main components instead of CO₂. The conversion of lignin appeared to occur in two stages; first gasification of the solids and then reaction in between the gas species, mainly by the water gas shift reaction⁴. The first stage takes place during the first 2.5 minutes while the second one occurs at longer reaction times. The yield of H₂, CH₄ and CO₂ increased with temperature, while the yield of CO decreased with temperature. Hence, high temperatures are important to achieve good gas yields. From varying the lignin loading, it was found that the lowest gas yields were obtained from the base case. Both higher and lower loadings gave higher yields for H₂, CH₄, CO₂ and total gas yield. For CO, on the other hand, the yield decreased with increasing loading. The CH₄/H₂ ratio also decreased with increasing lignin loading. The water density was also varied during the experiments. One density lower and one higher than the base case were evaluated, as well as one pyrolysis experiment with no water added. The pyrolysis gave lower yields for all components except CO than the SCWG experiments. The yield of CO was highest for the pyrolysis and decreased with increasing water density. For the other components and the total yield, the base case gave lower yields than the other two SCWG experiments. The highest yields were found for the highest density. In general, high temperature, water density and lignin loading should be used to achieve high total gas yield.

1.2.3 Pyrolysis of Lignin

A method for one-step conversion of lignin to biofuel has been investigated by Kleinert and Barth [10]. The method is called the lignin-to-liquid (LtL) process and the conversion is carried out by pyrolysis in two batch reactors made of stainless steel. The volumes of the reactors were 25 and 75 ml respectively. Lignin was added to the reactors together with formic acid and alcohol, which was used as hydrogen donating reaction medium. Water or DMC (dimethyl carbonate) was added in some cases. The reactors were heated in an oven in periods between 2 – 54 hours and then cooled in an air stream after completed reaction time.

³ More information about supercritical water and its properties can be found in Section 2.1.

⁴ The water gas shift reaction can be written as: $CO + H_2O \rightarrow CO_2 + H_2$ [33].

Decanting was used for separation of the product and the aqueous phase was extracted with dichloromethane. The organic phases were then recombined and concentrated in reduced pressure of 0.1 bar, which gave a dark brown liquid. The used lignin contained some inorganic salts, however these were found mainly in the aqueous phase after the pyrolysis. Some properties of the LtL oil, like oxygen content, heating value and density, were comparably similar to petroleum products. The oxygen-rich carbohydrate fractions are already removed for lignin residue taken from ethanol production, which improves the elemental composition of the lignin. During the LtL process, oxygen is removed and hydrogen added. This gives the produced oil an elemental composition similar to crude oil.

Barth and Kleinert [11] have also compared some techniques for pyrolysis of biomass. One of the techniques was the lignin-to-liquid (LtL) process, which was mentioned in the previous paragraph. It was concluded that the volatility of the produced LtL oil was an intermediate between petrol and diesel, and thus suitable for use as fuel. The oils produced by biomass pyrolysis were compared considering the following criteria: high yield, low oxygen content, high heating value, no coke, physical properties, miscibility with hydrocarbon-fuels, low water solubility, good phase separation, acidity level and chemical stability. It was found that LtL oil had good values on all of the criteria. It was considered the best product of those compared in the analysis.

1.2.4 Hydrocracking of Lignin

A process for hydrocracking of lignin for production of phenol and benzene has been invented and patented by Huibers et al. [12]. The process is based on pulverized lignin as feedstock, which is mixed with oil produced in the process before it is mixed with hydrogen gas and fed to a catalytic hydrocracking reactor. Proposed catalysts are oxides of iron, cobalt, molybdenum, nickel or a combination of these on an alumina or silica support. The preferred reactor conditions are 370 – 440°C and 40 – 140 bar(g)⁵. The resulting light product stream is taken to a phase separation step. The gas phase from this separation consists of hydrogen and is purified by removal of sulfur and other impurities. The hydrogen is then recycled back to the process. The phase separation also yields a fuel oil where one part is used for mixing with the lignin, as described earlier, while the other part is taken out as a product. A third stream, containing monoaromatics, is taken from the phase separation. It is brought to a thermal hydrodealkylation step where hydrogen is added. The resulting liquid stream is separated giving benzene and phenol. An estimation, based on experimental results, is that the yields from lignin can be 20 wt% phenol, 14 wt% benzene, 13 wt% fuel oil and 29 wt% fuel gas.

Engel et al. [13] invented another process for hydrocracking of lignin, which was patented in 1987. The purpose of the invention is to convert lignin to phenols via liquefaction and depolymerization. Only non-basic lignin should be used in this process because a basic solution would discourage the reaction. A phenolic solvent is used to dissolve the lignin with a solvent to lignin ratio of about 1.5 – 2.5. This solution is then reacted with hydrogen in the

⁵ The temperature and pressure are recalculated from °F and psig.

presence of a catalyst. The catalyst consists of tungsten and a metal, e.g. nickel, on a support which should be mildly acidic and not contain any alkali metals. The preferred supports are e.g. silica-alumina and silica-alumina phosphate. It has been found that the reaction is benefitted by an amount of methanol and water in the solution. The hydrocracking is performed at a pressure between 35 – 240 bar and a desired temperature interval from 375 to 425°C. Mixing is important for contact between the different phases. The reaction time needs to be sufficient for the liquefaction of lignin and optimized for the yield of desired phenolics, about 0.3 – 3 hours. The process can be carried out batch-wise or at continuous operation. If continuous operation is used, a fluidized bed may be preferred over a fixed bed due to plugging.

1.2.5 Black Liquor Gasification

Black liquor gasification in supercritical water⁶ has been examined by Sricharoenchaikul [2]. The temperature, pressure, reaction time and concentration of black liquor were examined considering conversion and energy efficiency. Weak black liquor, with a moisture content of 81.4%, was used for the experiments. The reaction took place in a quartz capillary with an inner diameter of 1 mm and a length of 15 cm. The heating was provided by a fluidized bed vessel which was preheated to a set temperature. When the desired temperature was reached, the quartz capillary was immersed into the vessel, which initiated the experiment. After the reaction time was reached, the capillary was quenched to terminate the reaction. The obtained products were gas, char and tar. The char and tar separation was accomplished by solution in dichloromethane (DCM) and subsequent filtration. Tar was obtained after evaporation of the DCM. The product yield and carbon conversion did not show any dependence of pressure during the trials. For all studied operating conditions, higher yield of gas product were obtained for higher temperatures while, at the same time, the char and tar contents were reduced. The fraction of gaseous products did also increase with reaction time. The amount of heavier carbon containing gases decreased at longer reaction times due to secondary decomposition. It was also concluded that higher energy efficiency was obtained for samples of lower black liquor concentration. The gas was found to have a maximum energy content of 9.4 MJ/m³, which is satisfactory for use as a fuel gas.

The carbon distribution in char residue from gasification of black liquor at low pressure and high temperatures has been investigated in another study by Sricharoenchaikul, in collaboration with Frederick and Agrawal [14]. It was found that the amount of fixed carbon in the char can influence the time required for gasification. The sodium and sulphur content should be recycled since they are used as pulping chemicals. However, the alkaline metal salts acts as catalysts during the gasification. The experiments were performed in a laminar entrained-flow reactor, which provides rapid heating. Small fuel particles are fed into one end of the reactor together with primary gas while preheated secondary gas is fed to the other end of the reactor. The fuel particles are heated rapidly upon entering the reactor and after the determined residence time, they are brought to a collector where they are quenched. The

⁶ More information about supercritical water and its properties can be found in Section 2.1.

experiments were carried out both in oxidizing gas environments and pyrolysis at 700 – 1100°C and the reaction time was between 0.3 – 1.7 s. Both the total carbon and the carbonate content in the produced char were analyzed. The fixed carbon content was then calculated as the difference between total and carbonate carbon. The carbonate content in the char residue changed with temperature and residence time for the pyrolysis; at 700°C, it increased, at 800°C it increased at first and then decreased around 1 s. For both 900°C and 1000°C, the carbonate content decreased with residence time (slowly for 900°C and rapidly for 1000°C). This indicates that two reactions take place, one forming carbonate and one consuming it. The results show that most of the carbon in the black liquor can be gasified even at pyrolysis conditions, i.e. without any oxidizing gases. During the trials in oxidizing gas environment, the different gasification conditions did not have any effect on the result at the lower temperatures (700°C and 800°C). For 900°C, increased residence time gave more char carbon when water vapor was used as an oxidizing gas than for the pyrolysis or the addition of CO₂. At 700°C, the carbonate yield was higher when CO₂ or water vapor was present than for the pyrolysis. The overall trends for the carbonate formation did not change with different gasification conditions. The carbonate fraction increased and then decreased again with residence time. In general, higher temperature and longer residence time decreased the fixed carbon yield.

1.2.6 Pyrolysis of Black Liquor

The St Regis process for pyrolysis of spent pulping liquors is a patented invention by W. G. Timpe from 1973. It was based on a pyrolysis of pulping liquors, which is heated to about 255 – 370°C at a pressure of about 70 – 240 bar⁷. The expected products were vapor, a solid precipitate and an aqueous effluent. [15] The idea of the process was to remove carbon, in form of char, and leave the inorganic chemicals in an aqueous phase, which could be used for recycling of the pulping chemicals. A pilot plant was built, but the idea was eventually abandoned because of e.g. an unfavorable energy balance. [16]

In 1987, Gilbert and Cooper [16] investigated hydrolysis of black liquor. The liquors used in the experiments were both kraft hardwood and softwood black liquors. Soap and tall oil was recovered from the black liquor before the hydrolysis. The concentrated liquors were prepared by dilution. The pyrolysis was performed in a magnetically stirred autoclave, with a volume of 1 liter. It was externally heated by two electrical heaters. The reactions were carried out at temperatures between 260 – 380°C. The reactor was filled with 400 – 600 g of black liquor and the reactions were performed for one hour. After the reaction, the temperature was decreased below 100°C. The gaseous products were not recovered, but the char was separated from the filtrate and kept unwashed in order not to dissolve any precipitated materials. The char and filtrate were dried before the remaining solids were analyzed. Samples of char and filtrate were adjusted to pH 2 with the help of HCl and extracted twice with ethyl acetate. Char and filtrate oils were collected after evaporation in a rotary vacuum evaporator. The results showed that char formation can occur at temperatures

⁷ The temperature and pressure are recalculated from °F and psig.

below 320°C, but the yield increases between 320 – 330°C. The carbon concentration in the char also increased with temperature. The amount of sodium bound in the char increased with temperature and was higher for strong liquors than for weak ones. The amount of recovered sulphur was not as high as for the other compounds; there are probably some losses with the gaseous phase. It did also decrease with temperature for hardwood black liquor, while it reached a minimum at 330°C for softwood liquors. The oil yield was determined from the extraction of acidified char and filtrate mentioned earlier. At 270°C, only 20% of the extractable material was found in the char, but at high temperatures (about 350 – 370°C), the amount was as much as 85 – 90%. On a basis of total black liquor solids, the yield was about 10 – 15%. Various oil samples were analyzed by gas chromatography and some simple phenols were identified. Finally, it was concluded that above 320°C, it is more efficient to use softwood liquors than hardwood liquors for hydrolysis of carbon to char.

1.2.7 Hydrogenation of Black Liquor

An experimental investigation of hydrogenation of kraft black liquor has been carried out by Creasy and Covey [17]. The black liquor used in the experiments originated from batch kraft eucalyptus pulping. The liquor was diluted with water, to give a concentration of 15.8% black liquor solids. The experiments were performed in an autoclave with a volume of 1 liter. The idea was to use the water gas shift reaction⁸ (WGS reaction) as the source of hydrogen for the liquid phase hydrogenation. Sodium was used as a catalyst for the WGS reaction in all experiments. During the trials, the reactor was heated to 350°C which took about 45 minutes. The reaction rate of the pyrolysis is rather slow during the heating period, while the water gas shift reaction almost reaches equilibrium. There are some ways to make the reaction rates more equal; the CO can be added when 350°C has been reached or e.g. borax⁹ can be used as catalyst for the pyrolysis. An experimental design was constructed where experiments with and without borax was conducted, CO was added at 15°C, 350°C or not at all and the black liquor was kept at 350°C for 20 minutes or quenched directly. In total, 14 experiments were carried out. After each test, the product was acidified with HCl and filtrated. Both the retentate and the filtrate were extracted with 1,1,1,tri-chloro ethane. The solids from the retentate extraction composed the char fraction, while the extract from the filtrate was evaporated and the residue was added to the retentate extract. The oil fraction was formed by combining the two extract residues. The mean value of the specific energy value was 28.1 kJ/g for the chars produced and about 32.7 kJ/g¹⁰ for the oil. The tests without CO gave a low amount of oil, while the best yields were obtained when CO was added at 15°C. For those tests, the yield increased when the reaction was continued for 20 minutes at 350°C. However, for the tests where CO was added at 350°C, the additional 20 minutes did not give good yields. Altogether, the hydrogenation gave four products; a gas phase (CO₂ and H₂), an aqueous phase containing most of the original sulphur and sodium, char and oil which can be used as fuel. 30 – 50% of the fuel value was found in the aqueous phase, which can be used if

⁸ The water gas shift reaction can be written as: $CO + H_2O \rightarrow CO_2 + H_2$ [33].

⁹ Sodium tetraborate decahydrate.

¹⁰ The mean value is calculated from data in [17].

it is brought back to the weak black liquor for evaporation and finally incineration in the recovery boiler.

1.2.8 Catalytic Hydrotreating of Black Liquor Oils

Elliott and Oasmaa [18] have performed experiments in laboratory scale for evaluation of catalytic hydrotreating of black liquor oils. The oils were produced by the Technical Research Center of Finland (VTT) in a high pressure autoclave with a volume of 1 liter. About 500 g black liquor was mixed with 45 g of NaOH in the autoclave. Nitrogen was charged to a pressure of 1-2 bar before the reactor was heated to 350°C. The reaction was carried out for 30 minutes, before the reactor was cooled to a temperature of 25°C. The oil phase and aqueous phase were collected, while the gases were released. The produced oil contained some sodium, which can affect further processing. This catalytic hydrotreatment removes contaminants with the help of catalysts in a hydrogen rich atmosphere under pressure. Experiments were carried out with black liquor oils with sodium and sodium-free oils, which had been acid-washed. The catalysts used in the trials were; CoMo on alumina support and NiMo on both alumina and zeolite support. The most of the experiments were carried out at two temperature stages; first a stabilization step at 280°C for 35 minutes and then a hydrocracking step at 380°C for 65 minutes. The hydrotreatment resulted in a water phase, a gas phase and an oil phase. The oil was vacuum distilled and separated from the water phase. The oil contained mostly phenols, but also some hydrocarbons. The distillate residue contained catalyst, sodium salts and some low-volatile organics. It was found that a large amount of the sodium was in the water phase when extra water was added in the experiment. The primary oil yield varied between 64 and 87 wt%. Distillation of the sodium containing black liquor oils only gave a small amount of distillate oil compared to the acid-washed oils. Adding water to the experiments also resulted in a higher yield of distillate.

1.2.9 Remarks

Some different methods for production of renewable fuels from lignin and black liquor have been studied. The LignoBoost process extracts lignin from black liquor, which can be used for different purposes. Incineration will give energy, but there is also a potential for further processing to more profitable products like chemicals and motor fuels. The LignoBoost process is promising and since the product can be used for many purposes, the most useful area for this product needs to be found.

Gasification of lignin and black liquor has potential for production of biofuel. The main products are gas, char and tar. The produced gas can be used for further processing to liquid fuels. Black liquor gasification is a promising method which probably will be used to some extent in the future.

Pyrolysis of lignin and black liquor is another technique which has been studied here. This method has been shown to give fuel oils which are similar to petroleum products. These similarities indicate that the products are promising for replacement of regular oil products.

Fuel oils have also been produced by hydrocracking of lignin, hydrogenation of black liquor and hydrotreatment of black liquor oils.

The methods described in this section have some potential for production of liquid fuels. However, most of them give byproducts like char and tar. It would be desirable to achieve a method for direct conversion of lignin or black liquor to liquid fuels. The studied methods are also performed either at supercritical conditions or at temperatures or pressures below the critical point¹¹. Near critical conditions has not been evaluated in any of these methods. There are some advantages with water reactions at near critical conditions which are discussed further in Section 2.1.1.

This master's thesis will discuss catalytic hydrocracking at near critical water conditions. Near critical water will have different properties than both water above the critical point and water at low pressure and temperature. Therefore, it is of interest to examine a method constructed for near critical conditions. This could also be a method for further processing of lignin extracted with the LignoBoost process.

1.3 Objective

A research project for investigation of conversion of lignin or black liquor to liquid fuels has been proposed as cooperation between Metso Power AB and Chalmers University of Technology. The conversion is expected to be accomplished through catalytic hydrocracking at near supercritical water conditions. A high pressure and temperature reactor of pilot scale has been acquired by Metso Power AB and installed at Chalmers for this purpose.

The first step in the experimental work is to start up the reactor and tune the operation with water before experiments with lignin and alternatively black liquor will be conducted. The purpose of the master's thesis is to initiate the experimental work with the reactor. The thesis work will be mostly experimental and consist of two parts; running the reactor with water and running it with lignin. The aim is to achieve results of how to run and control the reactor, which can be used for further experimental work and research.

1.4 Outline of the Thesis

The master's thesis work is presented in this report, which is organized in seven chapters:

Chapter 1 introduces the work by giving a background to the subject. It also provides a state of art considering research within conversion of lignin and black liquor into energy and biofuel.

Chapter 2 describes the theory of supercritical water and its properties. This chapter also presents the experimental setup of the pilot scale plant and how the plant should be operated. Furthermore, the different experimental methods for the thermodynamic studies are described

¹¹ The critical point for water is 374°C and 221 bar.

here. Finally, a description of the conducted pump trials with lignin slurry is found in this chapter.

Chapter 3 gives the results obtained from the experimental work. First of all, the results from the thermodynamic studies with water and secondly, the pump trial results with lignin can be found in this chapter.

Chapter 4 presents an analysis of the obtained results. Heat balances are used to set up mathematical models for the three heated units; the storage tank, the preheater and the reactor. Moreover, control and regulation of the plant during operation is analyzed.

Chapter 5 gives a discussion of both the experimental results and the theoretical results from the mathematical modelling. Furthermore, the control and regulation of the heating units are discussed here.

Chapter 6 contains the conclusions obtained from the analysis and discussion.

Chapter 7 discusses what could be done in further research within this topic.

2 Experimental Methodology

The experimental work was carried out in an autoclave station manufactured by Mothes Hochdrucktechnik, Berlin. The reactor is designed for high pressures and temperatures up to 345 bar and 500°C respectively. This chapter presents the plant and its components together with the start up and shut down procedures. Furthermore, the experimental procedures are described here. The experiments were performed at high pressures and temperatures at which water exists in a nearly supercritical phase. Hence, a theoretical section about supercritical water and its properties can also be found in this chapter.

2.1 Supercritical Water

It is common knowledge that a fluid can exist in different phases depending on its temperature and pressure. The three phases solid, liquid and gas are well-known, but a fluid can also occur in a supercritical phase. Figure 2.1 shows the relation between temperature, pressure and the phase regions. The supercritical region is located at temperatures and pressures above the critical point. The critical temperature and pressure depends on the fluid. For water, the critical point is at a temperature and pressure of 374°C and 221 bar respectively. [19; 20]

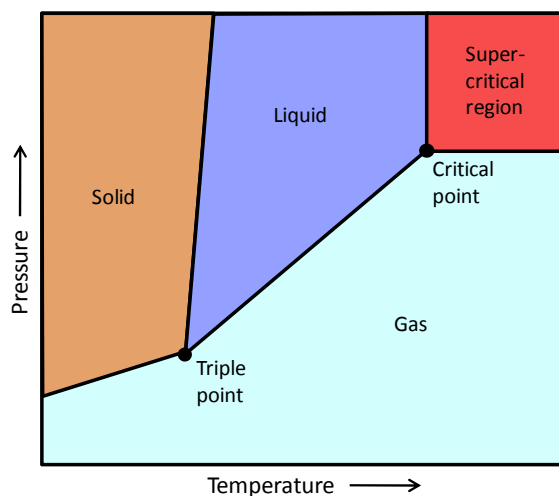


Figure 2.1. Phase diagram of a typical fluid. The different phases are separated by the solid lines. The supercritical region is located above the critical point.

As a fluid approaches the supercritical area, the phase transition between gas and liquid becomes less distinct. The fluids properties can be changed from liquid like to gas like without a phase transition by varying the temperature and pressure within the supercritical area. For supercritical water (SCW) the density increases with pressure. A high density gives more liquid like properties, while a low density corresponds to properties more similar to a gas. [20] If the density is decreased, the dielectric constant of SCW is also decreased due to breakage of hydrogen bonds. A decrease in the dielectric constant corresponds to a decrease in the polarity of water. Thereby, the reduced effect of hydrogen bonds also results in a change of the solubility properties. [19] For instance, SCW at low pressure can dissolve

nonpolar compounds while ionic substances are insoluble. At high pressures, on the other hand, water in the supercritical region acts more like liquid water and ionic compounds can be dissolved. The heat capacity for SCW varies with temperature and pressure over a wide range. It can be very high compared to “normal” water and steam. Furthermore, the dynamic viscosity depends on the temperature and density. For SCW at high density, it decreases with temperature while it increases with temperature for low density. [20] Due to high compressibility, the pressure needs to be accounted for when reactions are carried out in SCW. For instance, the reaction rate constant can be changed by varying the pressure. [19; 20]

2.1.1 Near Supercritical Water

The purpose of approaching the critical point but not exceeding it is to maintain the polarity of water while it at the same time becomes reactive. When the critical point is approached, the ionic product¹² of the water increases with temperature. A maximum value is reached at 300°C and then above the critical point, it decreases dramatically. [21] The polarity of water will thereby be remained at nearly supercritical conditions even if it less polar than water at room temperature [22]. The maximum value of the ionic product is caused by two competing phenomena. First of all, the density of water decreases with temperature. Decreasing density reduces water's ability to dissolve ions, which was mentioned in the previous section. On the other hand, dissociation of water into ions (H^+ and OH^-) is an endothermic process and the equilibrium constant is increased with temperature. [21] The reactivity of water increases when the critical point is approached [22]. Water may act as an acid or base catalyst due to the high ionic product. However, it has been found that the water may also function as a proton donor or acceptor in the reactions. Furthermore, salts can influence reactions by acting as an acid or a base in subcritical and supercritical water. [23] Water at nearly supercritical conditions has been used for conversion of biomass into liquid or gaseous fuels or to chemicals [21; 23].

2.2 Experimental Setup

The pilot scale plant consists of three main parts; a control unit, an educt box and the reactor module. The reactor can be operated both in continuous mode and as a batch reactor. In continuous mode, the maximum flow rate is 3 l/h.

The control unit contains the electrical cabinet and the regulators for the control equipment. Furthermore, switches for the heaters, mixers and the pump are located here. The control unit can be seen in Figure 2.2.

¹² The ionic product can be written as: $K_w = [H^+][OH^-]$.



Figure 2.2. The control unit.

The educt box contains a storage tank with a volume of 10 liter and a disc propeller for mixing of the raw material. Moreover, the temperature in the tank is controlled by an electrical heating jacket and measured by a thermocouple. The other main component of the educt box is a pump, which facilitates the flow in the system. The flow rate is measured by a mass flow meter and regulated by a frequency inverter. Furthermore, the raw material can be recirculated to the tank in order to secure the function of the pump. The pump also enables the pressure increase in the system which is displayed on a pressure gauge situated ahead of the flow meter. Figure 2.3 shows the educt box together with its components.



Figure 2.3. The educt box. The storage tank and the pump are the main components of the unit.

After the flow meter, the stream enters the reactor module and an electrical preheater, where the temperature can be raised up to 300°C. The outlet temperature is measured by a thermocouple before the stream enters the reactor. Further heating can be accomplished in the reactor, which is heated by an electrical heating jacket. A thermocouple is used to measure the temperature inside of the reactor. The design pressure and temperature of the reactor is 345

bar and 500°C. A cooling coil is installed in the reactor, which can be used to stop the reaction in batch mode by lowering the reactor temperature. However, it should not be used at elevated reactor temperatures due to sudden evaporation of the cooling water, which can result in high stress to the material. A stirrer driven by a magnetic coupling is used for mixing of the reactor, which has a volume of 0.5 liter. Both the reactor and the preheater are protected against excessive pressure by rupture discs, with a burst pressure of 350 bar. The pressure inside of the reactor is controlled by a pressure control valve, which is situated at the product outlet from the reactor unit. A gas phase stream can be removed from the reactor via a sampling tube. The liquid product stream is taken out by a dip tube and passed through a cooler in order to decrease the temperature of the fluid before samples can be collected. [24] The experimental setup can be seen in the process flow diagram in Figure 2.4.

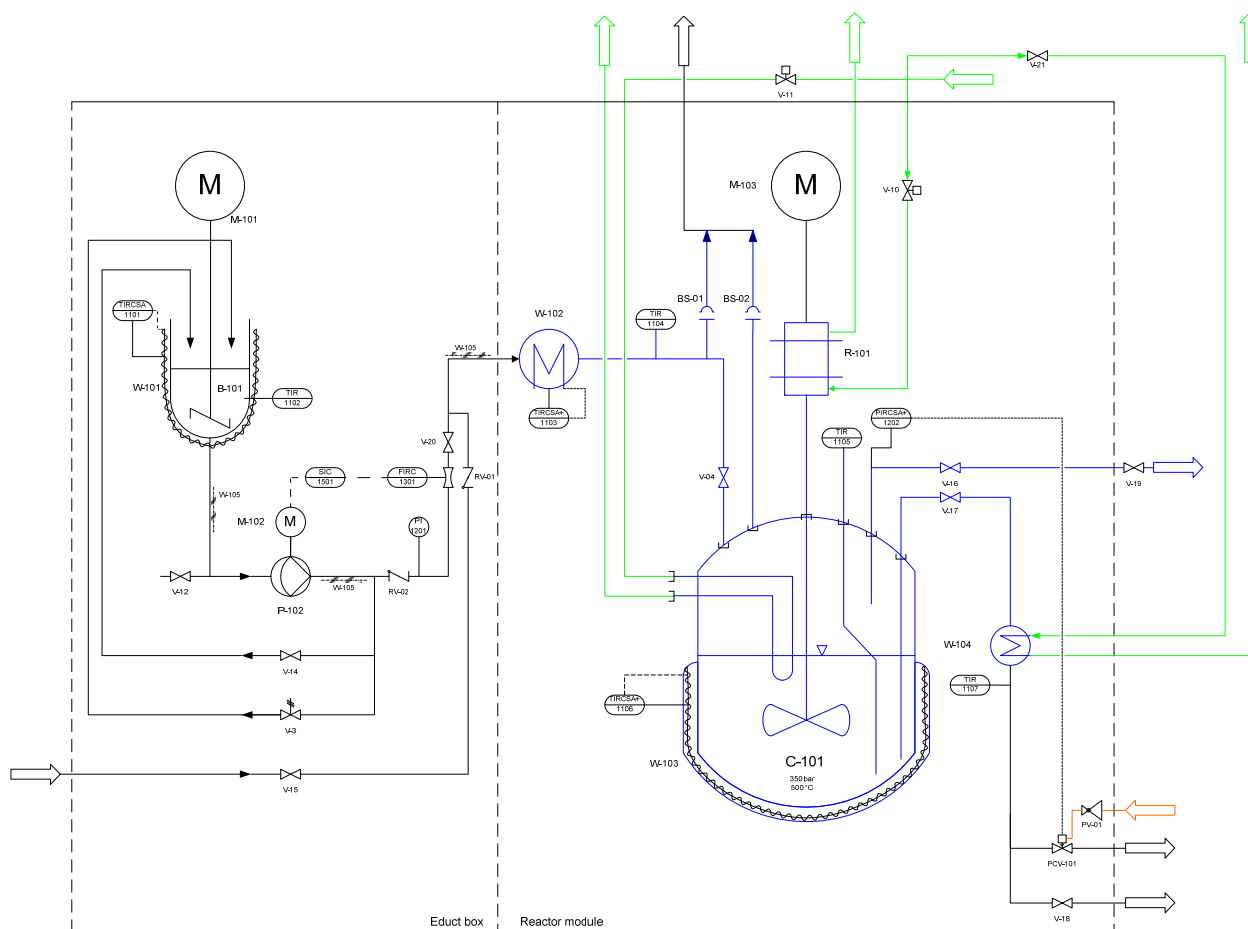


Figure 2.4. Process flow diagram of the reactor plant.

The reactor module is installed in a safety box lined with 4 mm thick sheets of aluminum. A safety glass pane is installed in the door so the interior of the reactor module can be inspected during operation. This can be seen in Figure 2.5. Both the educt box and the reactor module have connections for ventilation.

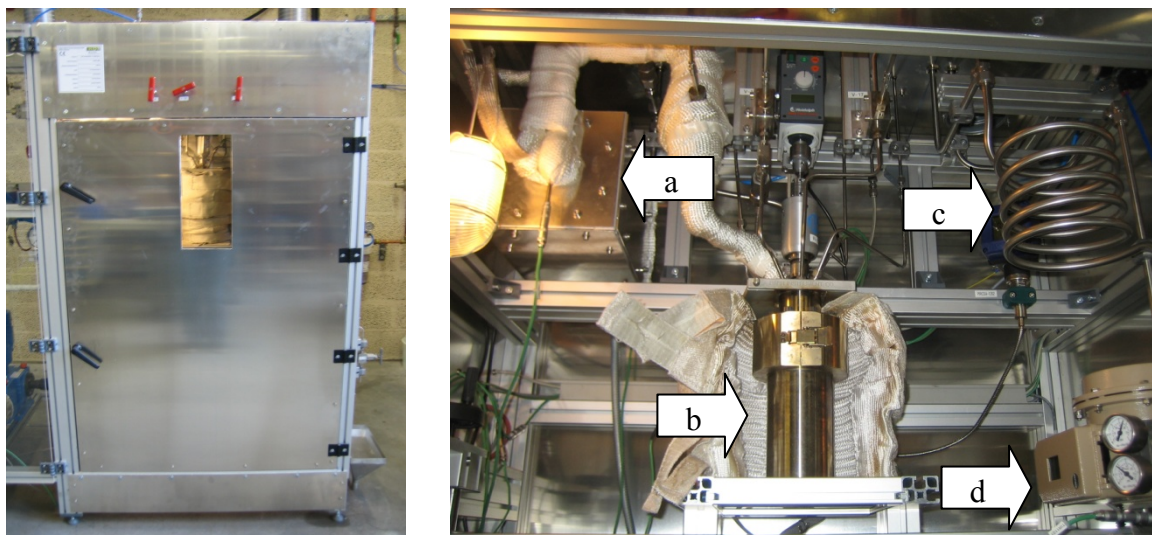


Figure 2.5. The reactor module. The left picture shows the outside with the aluminum door and safety glass pane. The picture to the right shows the interior of the module with the preheater (a), the reactor (b), the cooler (c) and the pressure control valve (d).

The standard material used for the piping is stainless steel. However, due to high pressure and temperature, Inconel 600 has been used for manufacturing of the preheater, reactor and cooler as well as the piping and other components in between. [24]

2.2.1 Safety Measures

The main risks with the pilot scale plant are due to the high pressure and temperature at which it operates. It is important to be aware of the risks and necessary safety measures before working with the plant. The high pressure could result in mechanical hazards due to bursting of plant components. Thus, the protective equipment should always be used when the plant is in operation. For instance, the door to the reactor module should be closed when the system is pressurized. High temperatures can give rise to thermal hazards such as burn damages from touching hot components. Therefore, the plant parts should not be touched during operation and the protective cover should always be in place. After running the plant, the hot parts should cool down before the cover is opened. Furthermore, the process chemicals used in the pilot plant should be considered with aspect to its effect on the equipment and health aspects. [24]

2.3 Operation of the Plant

To be able to operate the pilot scale plant, some knowledge about essential routines, like start up and shut down, is needed. These two procedures are described here for continuous operation.

2.3.1 Start Up

First of all, the power is turned on by pressing the on button. Then, the temperature limiter is switched on. To electrically activate the plant for operation, the start button is pressed. That cannot be done directly after the power is switched on, there is a waiting time about one minute before the start button can be pressed.

The compressed air should be available at 4 bar, there is an indication at the pressure control valve where this can be controlled. Nitrogen should be used to create an inert atmosphere in the reactor.

If preheating of the raw material is needed, the heating jacket to the storage tank can be switched on. Mixing is obtained by activating the stirrer. The four valves between the pump, preheater, reactor, cooler and the outlet should be closed and the valve which allows recirculation should be opened. The recirculation confirms the function of the pump.

The pump must be switched on in manual mode, since there needs to be a flow through the flow measurement for the automatic mode to be available. To allow flow through the reactor, the four valves mentioned earlier (between the pump and outlet) are opened and the recirculation valve closed. The pump can now be switched to automatic mode since there is a flow through the flow measurement that controls the pump.

Before pressurizing the system, the pressure control valve should be opened manually to 100%. The other outlet valve is closed at the same time. The pressure control valve can now be switched to automatic mode and the pressure set. The pressure will now rise to the desired value. Initially, there will be no flow from the pressure control valve due to the pressure build up.

The mixing in the reactor is obtained by switching on the magnetic stirrer. If it is activated, cooling should be activated by opening the magnetic valve that provides a cooling stream to the stirrer. This is done by a switch at the control panel. The cooler stream that cools down the product stream should also be enabled by opening the valve to the cooling water.

The heaters for piping, preheating and to the reactor can now be activated. The pressure should be high enough to avoid evaporation in the system, before the temperature is raised.

2.3.2 Shut Down

To start with, the heating system is turned off to allow temperature decrease in the system. When the temperature has decreased to a point where evaporation will not be obtained at atmospheric pressure, the pressure in the system can be decreased. It is done by first switching off the pump and then manually opening the pressure control valve. The valve should be opened slowly so the pressure is reduced gradually. Finally, the system should be purged with nitrogen.

2.4 Experiments with Water

The first step in the experimental work is to start up the reactor and tune the operation with water before experiments with lignin can be conducted. It is important to obtain knowledge of how the plant operates and its dynamics before experiments with reacting material are conducted. Therefore, thermodynamic studies of the heating components were performed.

2.4.1 Thermodynamic Study of the Storage Tank

The principle of the thermodynamic study of the storage tank was to heat up the tank from ambient temperature. Different set values of the heating jacket were chosen, which can be seen in Table 2.1. The time for the temperature of the water inside of the tank to reach steady state was then measured as well as the steady state temperature.

Table 2.1. The different temperatures which were set for the electrical heating jacket during the storage tank experiments.

Experiment number	Temperature of the electrical heating jacket
T1	50°C
T2	60°C
T3	70°C
T4	80°C

2.4.2 Thermodynamic Study of the Preheater

The preheater is a heat exchanger where the heat is supplied by a cartridge heater which is situated inside of an aluminum body. The water flows through a pipe which is wired into the aluminum. Figure 2.6 shows the interior of the preheater.



Figure 2.6. The interior of the preheater. The cartridge heater is situated in one of the tubes in the middle, the other one is a preparation for use of two cartridge heaters. The water pipe enters and leaves the aluminum to the left in the picture.

The thermodynamic of the preheater was studied by examining which temperature the cartridge heater needed to have in order to get a certain temperature of the water outlet stream. Three different temperatures, pressures and mass flow rates were chosen for the study. The experimental design can be seen in Table 2.2.

Table 2.2. Experimental design for the preheater experiments. Different temperatures, mass flows and pressures were examined.

Experiment number	Water temperature at outlet	Mass flow	Pressure
PH1	250°C	1 kg/h	150 bar
PH2	250°C	1 kg/h	175 bar
PH3	250°C	1 kg/h	200 bar
PH4	250°C	2 kg/h	150 bar
PH5	250°C	2 kg/h	175 bar
PH6	250°C	2 kg/h	200 bar
PH7	250°C	3 kg/h	150 bar
PH8	250°C	3 kg/h	175 bar
PH9	250°C	3 kg/h	200 bar
PH10	280°C	1 kg/h	150 bar
PH11	280°C	1 kg/h	175 bar
PH12	280°C	1 kg/h	200 bar
PH13	280°C	2 kg/h	150 bar
PH14	280°C	2 kg/h	175 bar
PH15	280°C	2 kg/h	200 bar
PH16	280°C	3 kg/h	150 bar
PH17	280°C	3 kg/h	175 bar
PH18	280°C	3 kg/h	200 bar
PH19	310°C	1 kg/h	150 bar
PH20	310°C	1 kg/h	175 bar
PH21	310°C	1 kg/h	200 bar
PH22	310°C	2 kg/h	150 bar
PH23	310°C	2 kg/h	175 bar
PH24	310°C	2 kg/h	200 bar
PH25	310°C	3 kg/h	150 bar
PH26	310°C	3 kg/h	175 bar
PH27	310°C	3 kg/h	200 bar

Due to large variations in the results between the two higher flow rates, 2 and 3 kg/h, three additional experiments were carried out with a flow rate of 2.5 kg/h. This can be seen below, in Table 2.3.

Table 2.3. Additional experiments for the thermodynamic study of the preheater.

Experiment number	Water temperature at outlet	Mass flow	Pressure
PH28	250°C	2.5 kg/h	200 bar
PH29	280°C	2.5 kg/h	200 bar
PH30	310°C	2.5 kg/h	200 bar

2.4.3 Thermodynamic Study of the Reactor

The reactor is heated by an electrical heating jacket, just like the storage tank. This heating jacket can be seen in Figure 2.7. It encloses the reactor according to the picture. The main difference between the storage tank and the reactor is that there is a flow entering and leaving the reactor. This influences the heating since the inlet will have a lower temperature than the inside of the reactor and thereby cool down the system.



Figure 2.7. The reactor with and without the electrical heating jacket on.

For the experimental investigation of the reactor, the required temperature of the heating jacket was found for a predetermined reactor temperature. This was done for different values of the mass flow and reactor inlet temperature while the pressure was kept constant at 200 bar. The experimental design can be seen in Table 2.4.

Table 2.4. Set values of mass flow and temperatures for all reactor experiments. The experiments were carried out at a pressure of 200 bar.

Experiment number	Temperature in reactor	Water temperature at inlet	Mass flow
R1	325°C	250°C	1 kg/h
R2	325°C	250°C	2 kg/h
R3	325°C	250°C	3 kg/h
R4	325°C	280°C	1 kg/h
R5	325°C	280°C	2 kg/h
R6	325°C	280°C	3 kg/h
R7	350°C	250°C	1 kg/h
R8	350°C	250°C	2 kg/h
R9	350°C	250°C	3 kg/h
R10	350°C	280°C	1 kg/h
R11	350°C	280°C	2 kg/h
R12	350°C	280°C	3 kg/h

To investigate if the pressure influences the heat transfer of the reactor, additional experiments were performed for R1 and R2 at different pressures.

2.5 Experiments with Lignin

After the test series with water, described in previous chapters, the experimental work was continued with lignin trials. First of all, the dry content of the lignin was evaluated and then, some pump trials at different lignin concentrations were performed.

2.5.1 Pump Trials with Lignin Slurry

Before the pump trials with lignin slurry were carried out, the dry content of the lignin was determined. The lignin was obtained from the Bäckhammar plant earlier described in Section 1.2.1. Four samples of about 12 g were collected, weighed and then dried in an oven overnight. The following day, they were cooled down to room temperature and weighed again. Hence, the amount of evaporated water could be obtained and the dry content calculated.

The lignin slurries were prepared to give predetermined weight percentages of lignin¹³. These different concentrations can be seen in Table 2.5.

Table 2.5. Concentration of lignin in the pump trials.

Experiment number	Lignin concentration in the slurry
L1	5 wt%
L2	10 wt%
L3	15 wt%
L4	20 wt%
L5	40 wt%

The slurry was mixed with an Ultra-Turrax disperser in order to dissolve all lignin into the water, which can be seen in Figure 2.8. Then, the slurry was poured into the storage tank and the valves opened and closed in order to obtain a recirculation back to the tank once the pump was started. The evaluation of the pump trials was simply if the pump could manage to recirculate the slurry or not.



Figure 2.8. Mixing of the lignin slurry.

¹³ The lignin from the Bäckhammar plant was used without any further preparation.

3 Results

This chapter presents the results from the conducted experiments. First the results from the thermodynamic studies of the storage tank, the preheater and the reactor. These were all carried out with water. Finally, the results from the lignin experiments are presented.

3.1 Experiments with Water

The experiments with water were carried out to get knowledge of the plant and its thermodynamic properties before trials were performed with lignin. In this section, the results from the thermodynamic studies of the equipment can be found.

3.1.1 Thermodynamic Study of the Storage Tank

During the experiments with the storage tank, the heating jacket was set to a predetermined temperature. The temperature of the water in the tank was then measured until the system had reached steady state. This is shown in Figure 3.1, where the temperature increase over time can be seen from the start of the experiment until the system had reached steady state.

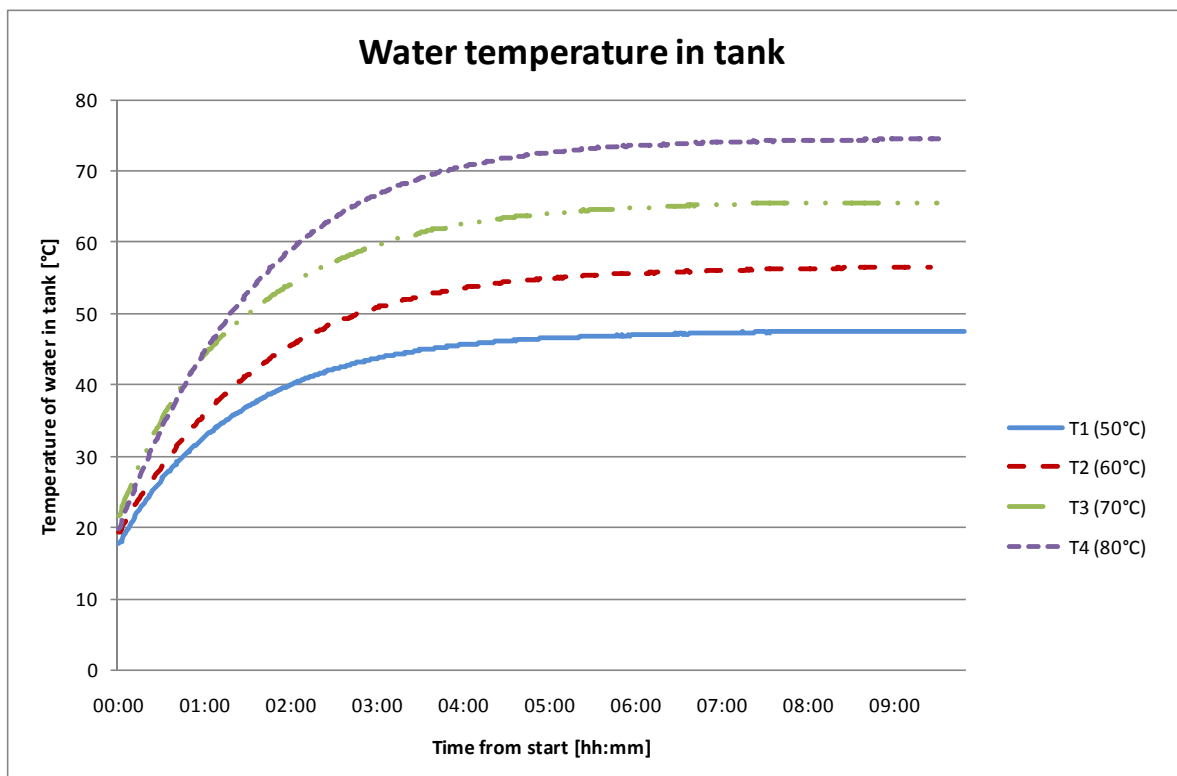


Figure 3.1. The temperature of the water inside of the storage tank plotted against the time from start for each set temperature of the heating jacket.

The results show that the temperature in the tank increases more rapidly at first, when the temperature difference between the heating jacket and the inside temperature are larger. When the temperature in the tank approaches its final value, the temperature increases less and less.

The final temperature of the water in the tank was measured and the results can be seen in Figure 3.2. It can be seen that the steady state temperature of the water is lower than the temperature of the heating jacket. That indicates that there are some heat losses in the system.

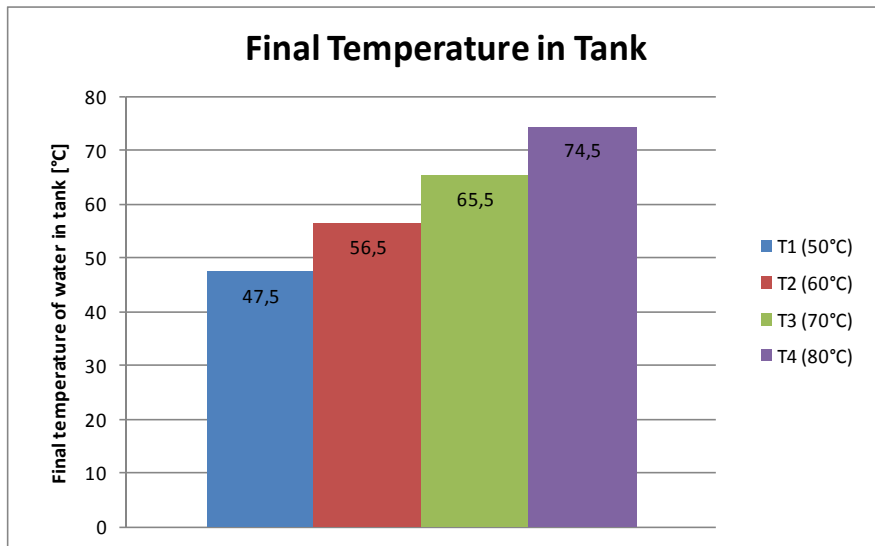


Figure 3.2. The final temperature of the water in the storage tank for all experiments.

To analyze the heat losses, the output in form of percentage of full effect to the heating jacket was noted during steady state. This output signal can be seen in Table 3.1 for each experiment. The heating jacket has a capacity of 2000 W, which means that an output of e.g. 50 % corresponds to an effect of 1000 W and so on.

Table 3.1. Output signal and the corresponding effect of the heating jacket for the different storage tank experiments.

Experiment number	Output signal	Effect of the heating jacket
T1	1%	20 W
T2	2%	40 W
T3	2.5%	50 W
T4	3.5%	70 W

3.1.2 Thermodynamic Study of the Preheater

During the study of the preheater, the temperatures of the aluminum and the cartridge heater were measured and the output signal noted. Like with the storage tank, the output corresponds to the percentage used of the full effect. Table 3.2 shows the results from all experiments with the preheater.

Data are missing for some of the experiments. That is because the pressure could not be controlled below 200 bar for the highest flow rate of 3 kg/h.

Table 3.2. All results from the experiments with the preheater. The pressure could not be regulated at pressures below 200 bar for a flow rate of 3 kg/h. Thereby, there are no data for 150 and 175 bar for the highest flow rate.

Experiment number	Water temp out	Aluminum temp	Temp of heater	Output
PH1	250°C	275°C	303°C	20%
PH2	250°C	275°C	303°C	20%
PH3	250°C	275°C	303°C	20%
PH4	250°C	276°C	310°C	32%
PH5	250°C	276°C	310°C	32%
PH6	250°C	275°C	313°C	33%
PH7	250°C	—	—	—
PH8	250°C	—	—	—
PH9	250°C	279°C	366°C	48%
PH10	280°C	310°C	346°C	24%
PH11	280°C	309°C	349°C	24.5%
PH12	280°C	309°C	350°C	24.5%
PH13	280°C	310°C	353°C	40%
PH14	280°C	309°C	352°C	40%
PH15	280°C	309°C	351°C	39%
PH16	280°C	—	—	—
PH17	280°C	—	—	—
PH18	280°C	315°C	411°C	57%
PH19	310°C	341°C	391°C	29%
PH20	310°C	341°C	391°C	28%
PH21	310°C	342°C	391°C	29%
PH22	310°C	342°C	415°C	48%
PH23	310°C	342°C	415°C	48%
PH24	310°C	342°C	416°C	48%
PH25	310°C	—	—	—
PH26	310°C	—	—	—
PH27	310°C	351°C	456°C	65%
PH28	250°C	276°C	352°C	40%
PH29	280°C	313°C	399°C	49%
PH30	310°C	348°C	442°C	57%

By studying the results in the table, it can be concluded that the pressure does not have any significant effect on the resulting temperatures and output. Experiments with the same desired temperature of the exiting water and the same flow rate give approximately the same results independent of the pressure. Therefore, pressure effects are not considered in further analyses of the results, which are based on the experiments performed at 200 bar.

Figure 3.3 shows a graphical representation of the preheater experiments at a pressure of 200 bar. The aluminum and cartridge heater temperatures are represented with dashed and continuous lines respectively. The temperatures are found on the y-axis and the mass flow of

water on the x-axis. The water outlet temperature is shown in brackets in the legend. There are three pairs of data, giving the aluminum and cartridge heater temperatures for each water temperature. These are given the same colors and symbols.

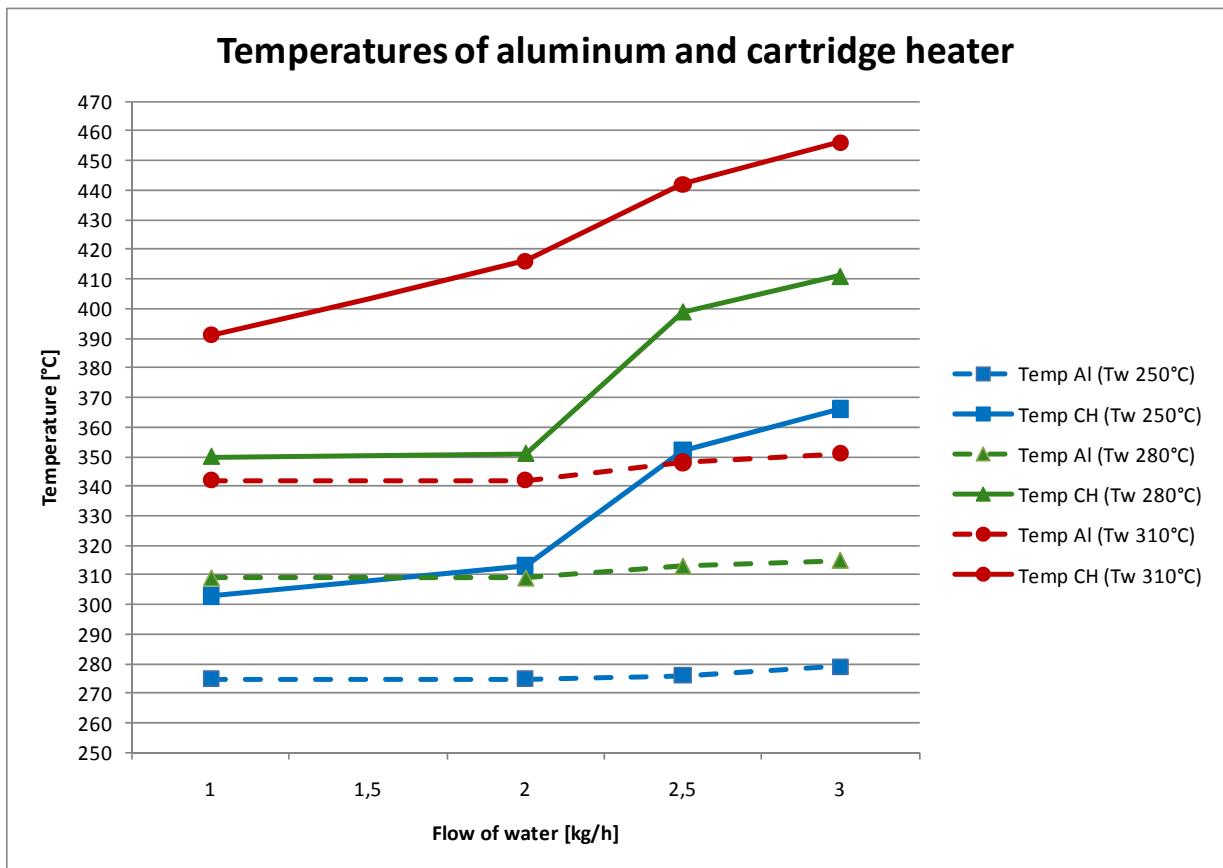


Figure 3.3. The temperatures of the aluminum and cartridge heater needed for different flow rates to obtain a temperature of the exiting water of 250°C, 280°C and 310°C respectively. All data is taken from experiments performed at 200 bar. The dashed lines represent the aluminum temperature and the continuous lines represent the temperature of the cartridge heater.

By studying the figure, it is obvious that the required temperature of the cartridge heater is strongly dependent on the mass flow of water through the preheater. For the two highest mass flow rates (2.5 and 3 kg/h), considerably higher temperatures were needed than for the lower flow rates. Furthermore, it can be seen that the required temperature of the cartridge heater increases a lot when the flow rate is increased from 2 kg/h to 2.5 kg/h. The increase between 2.5 and 3 kg/h is not as high. In total, the increase in heater temperature from the lowest to the highest flow rate is above 60°C in some cases.

It can also be seen that the temperature of the aluminum does not vary as much with the flow rate as the temperature of the cartridge heater does. The increase in aluminum temperature is lower than 10°C for all temperatures of the exiting stream. However, by studying the value of the output signal shown in Table 3.2, it can be seen that the higher flow rates requires a higher output signal even if the aluminum temperature is more or less unchanged. Moreover, higher temperatures are required to obtain a higher water outlet temperature.

3.1.3 Thermodynamic Study of the Reactor

The reactor experiments aimed at finding the required temperature of the heating jacket, which gave a desired temperature inside of the reactor. Furthermore, the wall temperature on the outside of the reactor was measured as well as the output signal to the heating jacket, which corresponds to the effect. All the results can be seen in Table 3.3 below.

Table 3.3. All results from the reactor experiments. The wall temperature and the temperature of the heating jacket were measured and the output signal to the heating jacket was noted for different temperatures in and out of the reactor.

Experiment number	Temp reactor	Inlet temp	Wall temp	HJ temp	Output
R1	325°C	250°C	339°C	427°C	33%
R2	325°C	250°C	346°C	468°C	43%
R3	325°C	250°C	354°C	508°C	55%
R4	325°C	280°C	338°C	419°C	30%
R5	325°C	280°C	345°C	444°C	38%
R6	325°C	280°C	350°C	471°C	46%
R7	350°C	250°C	366°C	462°C	38%
R8	350°C	250°C	376°C	515°C	54.5%
R9	350°C	250°C	389°C	563°C	72.5%
R10	350°C	280°C	365°C	457°C	37%
R11	350°C	280°C	375°C	494°C	49%
R12	350°C	280°C	383.5°C	536°C	63%

The results were also displayed graphically in Figure 3.4. The temperatures of the heating jacket and the outside of the reactor wall are plotted against the mass flow. These are represented with continuous and dashed lines respectively. In the legend, the inlet temperature of the water and the reactor temperature are found within brackets. In that way, there are four pairs of operating conditions, each giving one wall temperature and one temperature of the heating jacket. These have the same color and symbol.

There are some trends which should be noted in Figure 3.4. Higher temperatures on the heating jacket and the reactor wall are required for colder water inlet temperature, higher reactor temperature and higher mass flow. Furthermore, higher mass flow corresponds to a larger difference between the heating jacket temperature and the wall temperature. It can be seen in the figure that the incline is greater for the heating jacket curve than the corresponding curve for the wall temperature.

Moreover, the water inlet temperature does not seem to affect the wall temperature as much as the temperature of the heating jacket. The difference in wall temperature is not as great as the difference in heating jacket temperature for the two inlet temperatures. It can also be noted that the temperature difference is larger between the heating jacket and the wall than between the wall and inside of the reactor.

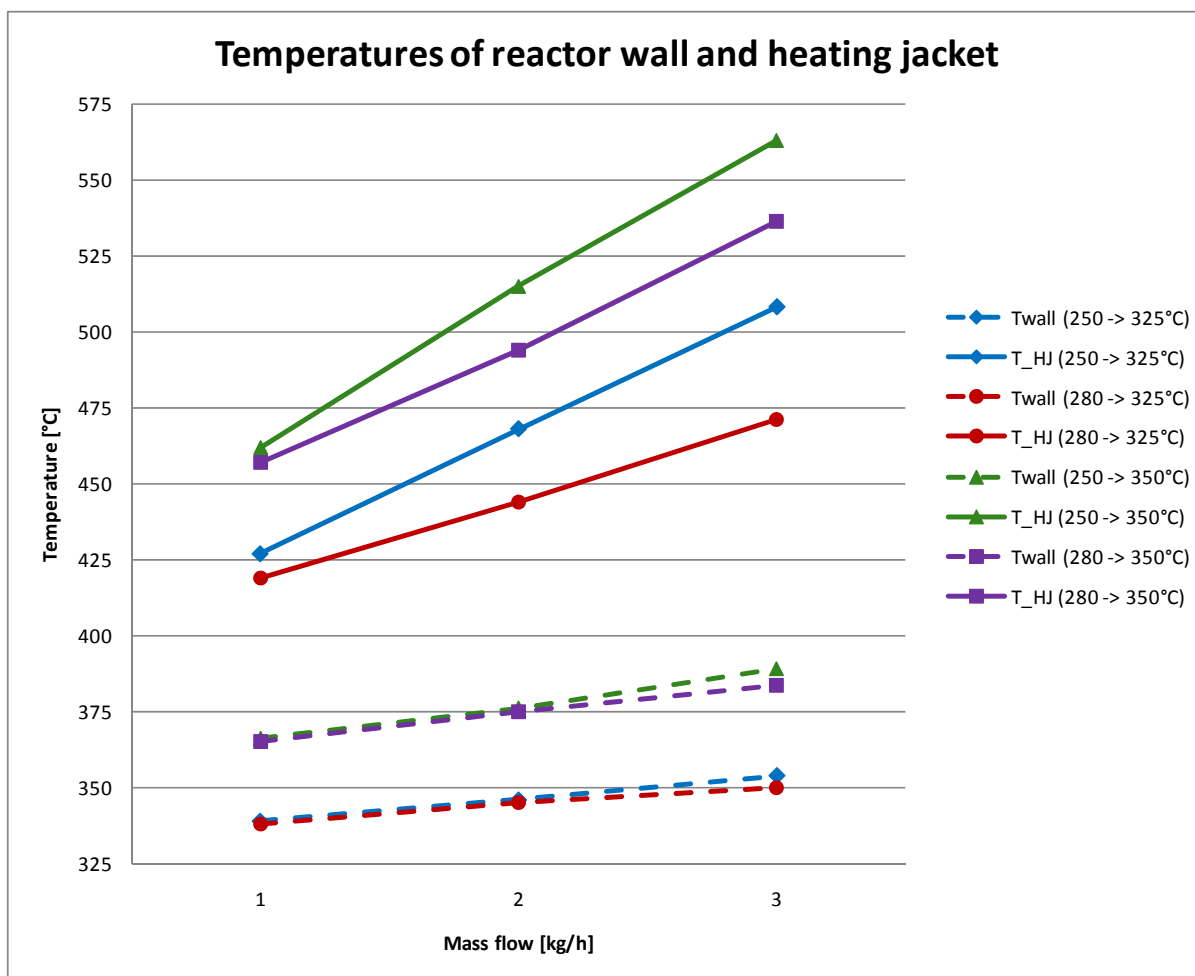


Figure 3.4. The results from the reactor experiments. The dashed and continuous lines represent the temperature on the outside of the reactor wall and of the heating jacket respectively. The water inlet temperature and reactor temperature are shown within brackets.

Since the pressure did not seem to have any significant effect on the preheater experiments, it was assumed that it would not affect the heat transfer in the reactor either. So the reactor experiments were all carried out at a pressure of 200 bar. Nevertheless, this assumption was investigated by changing the pressure for two of the test points, R1 and R2 in Table 3.3. These two were run at 150 and 175 bar in addition to the previous experiment at 200 bar. The result showed only a minor difference, which can be neglected. Thus, the assumption is validated.

During the reactor experiments, it was noted that the temperature of the cartridge heater, which supplies the heat in the preheater, needed to be higher than it was during the preheater experiments. This will be discussed further in Section 5.1.

3.2 Experiments with Lignin

This chapter contains the results from the pump trials with lignin slurry, which were carried out after the experiments with water were finalized.

3.2.1 Pump Trials with Lignin Slurry

The dry content of the lignin was investigated before it was used in the pump trials. Four samples were collected and evaluated. The mean value of the dry content for these four samples was 69 wt%.

During the pump trials, the prepared lignin slurry was recirculated to the storage tank. The behavior of the pump was then studied. If it would operate with proper recirculation and without any indications of overload, the trial would be considered as succeeded.

The first trial, with 5 wt% lignin in the slurry (L1), was succeeded. The lignin slurry was recirculated properly to the tank.

The second pump experiment, with 10 wt% lignin (L2), was also succeeded. The pump managed to recirculate the lignin slurry to the tank.

During the two trials with 15 and 20 wt% lignin (L3 and L4) the slurry was recirculated to the tank. However, several times the flow was interrupted and then continued again after some time. There are two non-return check valves situated at the inlet and outlet of the pump. They are each constructed with a small ball, which at the inlet is lifted up when the pump drags in the flow. Then when the fluid is pressed out, the ball should fall down and stop the flow from returning. Similarly, at the outlet, the ball is lifted up when the flow is pressed out and then it falls down to seal when the pump drags in new fluid to the pump house. In this case, there was probably some particle stuck underneath one of the balls, resulting in bad sealing of the check valve. Thereby, the flow would only go back and forth in the pump rather than passing through it. Since the flow was interrupted, the pump did not operate totally continuous and the trials may therefore not be considered as succeeded.

The fifth experiment, with 40 wt% lignin in the slurry (L5), failed. There was no flow back to the tank when the pump was switched on. The pump was stopped and the check valves at both the inlet and outlet were removed and cleaned. Then the pump was tested with water, which it could recirculate. Though, when a new trial with 40 wt% lignin was attempted, the same thing occurred once more. The valves were probably contaminated and the ball unable to seal from returning flow.

4 Analysis of the Results

In order to analyze the results from the experiments and to get a deeper knowledge of the dynamics in the system, mathematical models were set up for the three heated units; the storage tank, the preheater and the reactor. Furthermore, the control and regulation of the system were examined by studying the behavior of the system.

4.1 Mathematical Modelling

Heat balances were used for the mathematical modeling of the heated units mentioned above. The models aim to describe the system with heating of the water and losses to the surroundings.

4.1.1 The Storage Tank

The principle used for the heat balance of the water in the storage tank was:

Accumulated = Heating – Losses

This can also be written as:

$$\frac{dE}{dt} = Q_H - Q_{L1} \quad (4.1)$$

where

$\frac{dE}{dt}$ Energy accumulated in the water per time unit [W]

Q_H Heat transfer to the water from the heating jacket [W]

Q_{L1} Heat losses to the surroundings from the tank top [W]

Some assumptions were made for this heat balance. For instance, the heating jacket and ambient temperatures were assumed to be constant throughout the experiments. In addition, it was assumed that no energy was provided to the water in form of kinetic energy from the stirrer.

A sketch of the preheating tank can be seen in Figure 4.1. The temperatures of the heating jacket, the water and the ambient temperature are indicated in the figure as well as the heat flows.

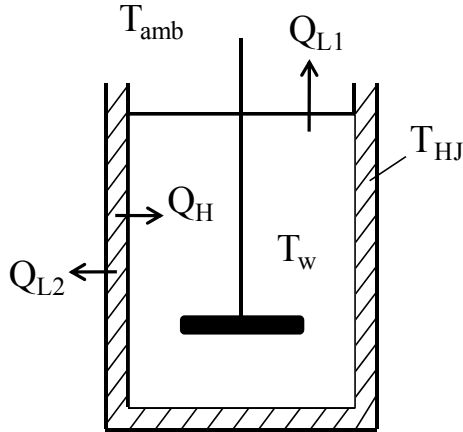


Figure 4.1. Sketch of the preheating tank with heat flows and temperatures marked on the drawing.

The time derivative of the energy taken up as heat by the water can be expressed as:

$$\frac{dE}{dt} = \rho V C_p \frac{dT_w}{dt} \quad (4.2)$$

where

ρ Density of the water [kg/m³]

V Volume of the water in the tank [m³]

C_p Heat capacity of the water [J/kgK]

$\frac{dT_w}{dt}$ Time derivative of the water temperature [K/s]

The heat accumulation in the water is due to heat transfer from the electric heating jacket to the water. The heating jacket temperature is controlled by an output signal to the heating jacket. This output signal corresponds to an effect, and can be found in Table 3.1 for each of the tank experiments. However, there are some losses to the surroundings, which can be described by equation 4.3:

$$P = Q_H + Q_{L2} \quad (4.3)$$

where

P Effect of the heating jacket [W]

Q_{L2} Heat losses from the heating jacket to the surroundings [W]

The heat transfer from the heating jacket to the water and the corresponding temperature profile can be seen in Figure 4.2.

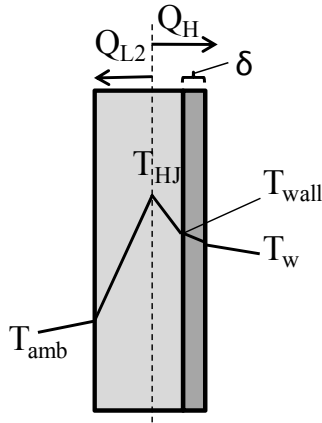


Figure 4.2. The temperature profile over the heating jacket and the tank wall. The heating jacket is indicated with light grey color and the tank wall with darker grey.

The highest temperature is found at the heat source inside of the heating jacket. This temperature is measured and denoted as T_{HJ} . Heat is then transferred to the tank wall and in to the water in the tank. At the same time, some heat is lost to the outside of the heating jacket. The heat transfer to the water can be divided into three parts; transport to the tank wall, transport through the tank wall and transport of heat in the water inside of the tank. If the system is in steady state, these three will be equal.

The heat transfer coefficient for the stirred water inside of the tank can be calculated according to [25 p. 958]:

$$Nu = C \cdot Re^a \cdot Pr^b \cdot \left(\frac{\mu}{\mu'}\right)^c \quad (4.4)$$

$$Nu = \frac{h_w D}{k_w} \quad (4.5)$$

$$Re = \frac{ND^2 \rho}{\mu} \quad (4.6)$$

$$Pr = \frac{\mu C_p}{k_w} \quad (4.7)$$

where

Nu Nusselt number [-]

Re Reynolds number [-]

Pr Prandtl number [-]

μ Dynamic viscosity of the water [Pas]

μ' Dynamic viscosity of the water at the tank wall [Pas]

h_w Heat transfer coefficient of the water [W/m²K]

D Agitator diameter [m]

k_w Thermal conductivity of the water [W/mK]

N Agitator speed [rps]

and C , a , b and c are constants.

It is assumed that the viscosity at the tank wall is equal to the viscosity of the water, which gives:

$$\left(\frac{\mu}{\mu'}\right)^c = 1 \quad (4.8)$$

Thereby, this term can be neglected in further calculations.

The mean values of the density, viscosity, heat capacity and thermal conductivity between 20 and 75°C can be found in the literature [26]. They can be seen in Table 4.1 together with the parameters for the agitator.

Table 4.1. Values of parameters used for calculation of the heat transfer coefficient of the water inside of the storage tank.

Parameter	Value	Unit
ρ	985	kg/m ³
μ	0.0005	Pas
C_p	4181	J/kgK
k_w	0.65	W/mK
D	0.1	m
N	2.17	rps

The value of the constants C , a and b depend on the type of agitator, if baffles are used or not and if the heat is transferred to the vessel wall or to coils. These values can be found in the literature [25 p. 959]. The heat transfer coefficient of the water was calculated for three different sets of constant values¹⁴. The resulting values of the heat transfer coefficient were 6500 – 7800 W/m²K. This indicates good heat transfer and the temperature in the water can hence be considered to be constant.

Furthermore, the transport of heat through the tank wall can be calculated with the equation for conductive heat transfer according to:

$$Q_H = \frac{k_{SS}}{\delta} A_{HX} (T_{wall} - T_w) \quad (4.9)$$

where

k_{SS} Thermal conductivity of the tank wall [W/mK]

δ Tank wall thickness [m]

¹⁴ The calculations for the water heat transfer coefficient can be found in Appendix A – Storage Tank Calculations.

A_{HX}	Heat exchanger area, i.e. the surface area of the tank [m ²]
T_{wall}	Temperature of the outside of the tank wall [K]
T_w	Temperature of the water [K]

Since the value for k_{ss} can be found in the literature [27] and the wall thickness is known (see Table 4.2), a heat transport value corresponding to the one calculated for the water can be found.

Table 4.2. Thickness and thermal conductivity of the tank wall.

Parameter	Value	Unit
δ	0.004	m
k_{ss}	16.5	W/mK

This corresponding heat transfer coefficient for the tank wall can now be calculated according to equation 4.10:

$$h_{ss} = \frac{k_{ss}}{\delta} \quad (4.10)$$

where

h_{ss} Heat transfer coefficient for the tank wall [W/m²K]

The resulting heat transfer coefficient is $h_{ss} = 4100$ W/m²K. Thus, the heat transfer in the tank wall is also very high and the temperature can be considered constant through the wall. Hence, the tank wall temperature must be equal to the water temperature in the tank. Thereby, the main heat transfer resistance must be found between the heating jacket and the tank wall.

First, the heat transferred to the wall from the heating jacket is assumed to be a combination of radiant heat transfer and convection/conduction through the jacket material according to equation 4.11. The dominating resistance can be found by comparing the magnitude of these terms.

$$Q_H = \epsilon \sigma A_{HX} (T_{HJ}^4 - T_w^4) + h_{HJ} A_{HX} (T_{HJ} - T_w) \quad (4.11)$$

where

ϵ Emissivity of the tank wall surface [-]

σ Stefan-Boltzman constant [W/m²K⁴]

T_{HJ} Temperature of the heating jacket [K]

h_{HJ} Heat transfer coefficient of the heating jacket [W/m²K]

Since the value for the emissivity can be found in the literature and the two temperatures are measured, the heat transfer coefficient is the only unknown parameter in equation 4.11.

The heat transfer coefficient can be estimated by using the fact that the losses to the surrounding, Q_L , are nearly zero from start when the tank is heated up from ambient temperature. Combining equations 4.1, 4.2 and 4.11 and assuming $Q_L = 0$ gives:

$$\rho V C_p \frac{dT_w}{dt} = \epsilon \sigma A_{HX} (T_{HJ}^4 - T_w^4) + h_{HJ} A_{HX} (T_{HJ} - T_w) \quad (4.12)$$

Since the tank is heated together with the water and the temperature of the tank wall is assumed to be the same as the water temperature, the first term in equation 4.12 includes both the tank and the water according to:

$$\rho V C_p = \rho_w V_w C_{p_w} + \rho_{ss} V_{ss} C_{p_{ss}} \quad (4.13)$$

where the index w corresponds to water and ss to stainless steel, which is the tank material. These values are assumed to be constant during the storage tank experiments since the temperature only varies between 20 and 75°C. Therefore, mean values for this temperature interval are used. The parameters for water [26] and stainless steel [27 p. 723] can be found in the literature as well as the value of ϵ [28 p. Ka3] and σ [27 p. 209]. Table 4.3 shows the values of these parameters.

Table 4.3. Values of the parameters used for calculation of the heat transfer coefficient of the heating jacket.

Parameter	Value	Unit
ρ_w	985	kg/m ³
V_w	0.009	m ³
C_{p_w}	4181	J/kgK
ρ_{ss}	7820	kg/m ³
V_{ss}	0.001145	m ³
$C_{p_{ss}}$	460.8	J/kgK
ϵ	0.69	—
σ	5.68E-08	W/m ² K ⁴

The heat exchanger area can be calculated from the diameter and height of the tank according to:

$$A_{HX} = \pi D_o H \quad (4.14)$$

where

D_o Outside diameter of the tank [m]

H Height of the tank [m]

Table 4.4 presents the dimensions of the tank together with the calculated heat exchanger area.

Table 4.4. Dimensions of the storage tank and the calculated heat exchanger area.

Parameter	Value	Unit
D_o	0.168	m
H	0.5	m
A_{HX}	0.264	m ²

The radiant heat transfer and the accumulated heat terms in equation 4.12 can now be calculated and compared. It was found that the radiant heat transfer accounts for 15 - 20% of the total accumulated heat. Neglecting the radiant term in equation 4.12 and assuming a total heat transfer coefficient gives:

$$\rho V C p \frac{dT_w}{dt} = h_{tot} A_{HX} (T_{HJ} - T_w) \quad (4.15)$$

where

h_{tot} Total heat transfer coefficient [W/m²K]

The total heat transfer coefficient of the heating jacket can now be calculated from equation 4.15 for each experiment. The resulting mean value for these cases was then calculated, giving $h_{tot} = 27$ W/m²K.

The heating equation of the storage tank is now determined and equation 4.11 can be written as:

$$Q_H = h_{tot} A_{HX} (T_{HJ} - T_w) \quad (4.16)$$

However, the heat losses to the surroundings should also be modeled. The losses are divided into two terms; losses from the tank top (Q_{L1}) and losses from the heating jacket (Q_{L2}).

The amount of heat lost to the surroundings from the top of the tank can be estimated with:

$$Q_{L1} = h_{L1} A_{cs} (T_w - T_{amb}) \quad (4.17)$$

where

h_{L1} Overall heat transfer coefficient to the surroundings [W/m²K]

A_{cs} Cross section area of the tank [m²]

T_{amb} Ambient temperature [K]

At steady state, when the temperature in the tank is constant. The heating term must equal the losses from the top of the tank according to:

$$Q_H = Q_{L1} \quad (4.18)$$

The cross section area can be calculated from the diameter of the tank:

$$A_{cs} = \frac{\pi D_0^2}{4} \quad (4.19)$$

The calculated value of the cross sectional area and the ambient temperature can be found in Table 4.5.

Table 4.5. The cross sectional area and ambient temperature used for calculation of the overall heat transfer coefficient to the surroundings.

Parameter	Value	Unit
A_{cs}	0.022	m ²
T_{amb}	20	°C

Since the heat flow to the tank can be calculated from equation 4.16 and the area and temperatures at steady state are known, the heat transfer coefficient from the top of the tank can be calculated. The mean value of this coefficient is: $h_{L1} = 34 \text{ W/m}^2\text{K}$.

This value can be compared with the convective heat transfer coefficient for free convection of air which is $5 - 50 \text{ W/m}^2\text{K}$ [27 p. 208].

Furthermore, the losses from the heating jacket to the surrounding can be described with:

$$Q_{L2} = h_{L2} A_{HJ} (T_{HJ} - T_{amb}) \quad (4.20)$$

where

h_{L2} Overall heat transfer coefficient to the surroundings [$\text{W/m}^2\text{K}$]

A_{HJ} Heating jacket area [m^2]

The heating jacket area can be calculated from the height of the tank and the outside diameter of the heating jacket according to:

$$A_{HJ} = \pi D_{HJ} H \quad (4.21)$$

where

D_{HJ} Outside diameter of the heating jacket [m]

The value for the heating jacket diameter and the resulting area can be found in Table 4.6 below:

Table 4.6. The outside diameter and area of the heating jacket.

Parameter	Value	Unit
D_{HJ}	0.24	m
A_{HJ}	0.38	m ²

By combining equations 4.3 and 4.20 at steady state, the heat transfer coefficient for the losses from the heating jacket can be calculated. The resulting mean value is: $h_{L2} = 1.1 \text{ W/m}^2\text{K}$.

This can be compared to conduction through a 3.5 cm thick insulation material which is about $1.1 - 2.4 \text{ W/m}^2\text{K}^{15}$ depending on the material.

4.1.2 The Preheater

The preheater was also evaluated with a heat balance. Figure 4.3 shows a sketch over the cross section of the preheater where the heat flows and temperatures are indicated. The cartridge heater and the aluminum are represented with dark and light grey color respectively.

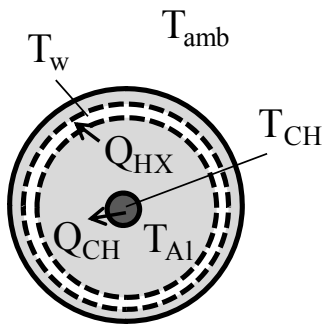


Figure 4.3. Cross section of the preheater. The dark grey section represents the cartridge heater, the light grey section the aluminum and the white section the water pipe. The heat flows and the temperatures are indicated in the picture.

For the modeling of the preheater, it is assumed that the temperature of the cartridge heater corresponds to the temperature in its stainless steel core and that it is constant. It is also assumed that the ambient temperature is constant and that the properties of the water inside of the preheater can be described with a mean value.

The results were analyzed by a heat balance over the preheater. The energy taken up by the water stream can be calculated by equation 4.22:

$$Q_w = \dot{m}(H_w^{out} - H_w^{in}) \quad (4.22)$$

where

Q_w Heat taken up by the water stream [W]

\dot{m} Mass flow of water [kg/s]

H_w^{out} Enthalpy of the water out from the preheater [J/kg]

H_w^{in} Enthalpy of the water in to the preheater [J/kg]

¹⁵ The value is calculated from the thermal conductivity $0.04 - 0.085 \text{ W/mK}$ [26].

The heat transferred from the aluminum to the water stream can be expressed with an equation for a heat exchanger according to:

$$Q_{HX} = UA_{HX}\Delta T_{lm} \quad (4.23)$$

where

Q_{HX} Heat transfer between the hot and cold side [W]

U Overall heat transfer coefficient [W/m²K]

A_{HX} Heat exchanger area [m²]

ΔT_{lm} Logarithmic mean temperature difference [K]

Furthermore, the logarithmic mean temperature is calculated with the temperature differences between the hot and cold sides (see Figure 4.4) according to:

$$\Delta T_{lm} = \frac{\Delta T_1 - \Delta T_2}{\ln\left(\frac{\Delta T_1}{\Delta T_2}\right)} \quad (4.24)$$

$$\Delta T_1 = T_{Al} - T_w^{in} \quad (4.25)$$

$$\Delta T_2 = T_{Al} - T_w^{out} \quad (4.26)$$

where

T_{Al} Temperature of the aluminum [K]

T_w^{in} Temperature of the water in to the preheater [K]

T_w^{out} Temperature of the water out from the preheater [K]



Figure 4.4. The temperature profile for the preheater. The temperature differences used to calculate the logarithmic mean temperature are also indicated in the figure.

The temperature of the water out from the preheater is measured in the experiments and thereby known. The temperature of the entering water, on the other hand, is not measured. However, during the preheater experiments water was taken from the storage tank in which the water temperature was about 40°C. On the way to the preheater, the water is cooled when passing the pump and the flow meter. Then again, there is electric tracing on the pipes between the tank and the preheater, which was set to a temperature of 80°C. It was assumed that the heat applied from the tracing was about enough to cover for the heat lost in the pump and flow meter. Thereby, the water entering the preheater was assumed to hold 40°C. In

addition, the aluminum temperature is assumed to be constant throughout the heat exchanger. This assumption will be evaluated later on in this modelling section.

The heat exchanger area between the aluminum and the water can be calculated according to:

$$A_{HX} = \pi D_i L \quad (4.27)$$

where

D_i Inside diameter of the water pipes [m]

L Length of the water pipe inside of the preheater [m]

The values of these parameters were known and can be found in Table 4.7 below together with the calculated area.

Table 4.7. The dimensions of the water pipes in the preheater and the heat exchanger area.

Parameter	Value	Unit
D_i	0.004	m
L	6	m
A_{HX}	0.075	m ²

Since the energy taken up by the water stream (Q_w) must be equal to the energy transferred from the aluminum to the water (Q_{HX}), an experimental value for the overall heat transfer coefficient, U_{expr} , can be calculated. The results clearly show that the overall heat transfer coefficient varies with the mass flow. On the other hand, the values did not vary almost anything with the temperature out from the preheater. Possible explanations for this will be discussed further in Section 5.2. The mean value of this experimental heat transfer coefficient was calculated for each mass flow, which can be seen in Table 4.8.

Table 4.8. The mean value of the experimentally calculated overall heat transfer coefficient for each mass flow.

Mass flow	Overall heat transfer coefficient, U_{expr}
1 kg/h	36 W/m ² K
2 kg/h	72 W/m ² K
2.5 kg/h	86 W/m ² K
3 kg/h	100 W/m ² K

The theoretical overall heat transfer coefficient, U_{theory} , depends on the heat transfer resistance in the aluminum, in the water pipe (which is made of Inconel 600) and in the water according to:

$$\frac{1}{U_{\text{theory}}} = R_{Al} + R_{Inc} + R_w \quad (4.28)$$

where

U_{theory} Theoretical overall heat transfer coefficient [W/m²K]

R_{Al} Thermal resistance in the aluminum [m²K/W]

R_{Inc} Thermal resistance in the Inconel [m²K/W]

R_w Thermal resistance in the water [m²K/W]

In order to find the dominating resistance, these three were calculated and compared.

The heat transfer coefficient for the water inside of the pipe can be calculated with dimensionless number correlations [28 p. Gb1] according to:

$$Re = \frac{\rho u D_i}{\mu} = \left\{ u = \frac{\dot{V}}{A_{cs}} = \frac{\dot{m}/\rho}{\pi D_i^2/4} = \frac{4\dot{m}}{\rho \pi D_i^2} \right\} = \frac{4\dot{m}}{\mu \pi D_i} \quad (4.29)$$

$$Pr = \frac{\mu C_p}{k_w} \quad (4.30)$$

$$Nu = 3.65 + \frac{0.19 \left(Re \cdot Pr \frac{D_i}{L} \right)^{0.8}}{1 + 0.117 \left(Re \cdot Pr \frac{D_i}{L} \right)^{0.467}} \quad (4.31)$$

$$Nu = \frac{h_w D_i}{k_w} \quad (4.32)$$

where

Re Reynolds number [-]

ρ Density of the water [kg/m³]

u Velocity of the water [m/s]

μ Viscosity of the water [Pas]

\dot{V} Volumetric flow [m³/s]

A_{cs} Cross sectional area of the pipe [m²]

Pr Prandtl number [-]

C_p Heat capacity of the water [J/kgK]

k_w Thermal conductivity of the water [W/mK]

Nu Nusselt number [-]

h_w Heat transfer coefficient for the water inside the pipe [W/m²K]

The resulting heat transfer coefficient was calculated to $h_w = 590 \text{ W/m}^2\text{K}$ ¹⁶. The heat transfer resistance is the inverse of this coefficient, which can be seen in equation 4.33:

$$R_w = \frac{1}{h_w} \quad (4.33)$$

Furthermore, the heat transfer resistance in the water pipe is due to conduction and can be calculated according to:

$$R_{Inc} = \frac{\delta_{Inc}}{k_{Inc}} \quad (4.34)$$

where

δ_{Inc} Thickness of the water pipe wall [m]

k_{Inc} Thermal conductivity of the water pipe [W/mK]

The heat transfer resistance in the aluminum is also due to conduction. However, the heat is supplied by a cartridge heater situated in the centre of the aluminum. The heat is then transferred radially to the water pipe. The heat exchange area used for calculation of the U-value and the rest of the heat transfer resistances will thereby not be the same as the area of heat exchange in the aluminum. The equation for this resistance will therefore include the ratio between the two areas according to [27 p. 213]:

$$R_{Al} = \frac{\ln\left(\frac{D_w}{D_{CH}}\right)}{2\pi k_{Al} L_{CH}} A_{HX} \quad (4.35)$$

where

D_w Diameter of the wiring of the water pipe [m]

D_{CH} Diameter of the cartridge heater [m]

k_{Al} Thermal conductivity of the aluminum [W/mK]

L_{CH} Length of the cartridge heater [m]

These dimensions can also be seen in Figure 4.5.

¹⁶ Calculations for the water heat transfer coefficient can be found in Appendix B – Preheater Calculations.

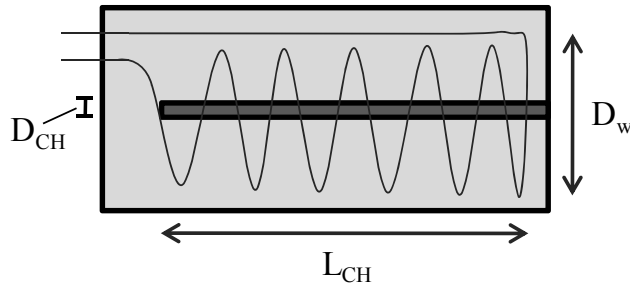


Figure 4.5. Sketch over the preheater where the dimensions of the cartridge heater are marked. It can also be seen how the water pipe is wired around the cartridge heater.

Values for the thermal conductivity for aluminum [27 p. 723] and Inconel [29] can be found in the literature. The thickness of the water pipe wall is known, while the dimensions of the cartridge heater and the aluminum were estimated from a picture of the preheater interior. Thereby, it is possible to calculate thermal resistances and the resulting values can be found in Table 4.9 together with the parameters used for the calculations.

Table 4.9. Values of the parameters used for calculation of the heat transfer resistances in the aluminum and the pipe wall and the calculated resistances.

Parameter	Value	Unit
δ_{Inc}	0.001	m
k_{Inc}	18	W/mK
D_w	0.1	m
D_{CH}	0.02	m
k_{Al}	230	W/mK
L_{CH}	0.2	m
R_w	0.00169	$\text{m}^2\text{K/W}$
R_{Inc}	0.0000556	$\text{m}^2\text{K/W}$
R_{Al}	0.000418	$\text{m}^2\text{K/W}$

By comparing the resistances, it is clear that the largest resistance lies within the water inside of the pipe. Furthermore, the thermal resistance in the aluminum is low enough to confirm that the previous assumption of constant temperature throughout the aluminum body is sufficiently accurate for these calculations. The theoretical U-value corresponding to these resistances is $U_{\text{theory}} = 460 \text{ W/m}^2\text{K}$.

It is obvious that there is a large difference between this calculated theoretical value of the heat transfer coefficient and the U-value calculated from the experimental data. Possible reasons for this deviation have been investigated and will be discussed in Section 5.2.

Heat is also being transferred between the cartridge heater and the aluminum. If the system is in steady state, the heat transfer between the cartridge heater and the aluminum must equal the heat transferred from the aluminum to the water, which is known. The cartridge heater consists of a core made of stainless steel with magnesium oxide around it and the heat transfer is modeled as radial conduction through the magnesium oxide according to:

$$Q_{CH} = \frac{2\pi k_{MgO} L_{CH}}{\ln\left(\frac{D_{CH}}{D_{SS}}\right)} (T_{CH} - T_{Al}) \quad (4.36)$$

where

k_{MgO} Thermal conductivity of the magnesium oxide [W/mK]

D_{SS} Diameter of the stainless steel core [m]

T_{CH} Temperature of the stainless steel core [K]

Equation 4.36 can be rewritten to substitute the term containing the thermal conduction and dimensions with a heat transfer coefficient and a heat exchange area, $(hA)_{CH}$:

$$Q_{CH} = (hA)_{CH} (T_{CH} - T_{Al}) \quad (4.37)$$

An experimental value for this constant can be calculated from equation 4.37. Since the value of the cartridge heater temperature varied between the preheater and reactor experiments, two values were calculated and compared. The resulting values are $(hA)_{CH, \text{expr, PH}} = 9.3$ W/K and $(hA)_{CH, \text{expr, R}} = 5.5$ W/K. This deviation will be discussed further in Section 5.1.

Moreover, a theoretical value can be calculated from equation 4.36 since the thermal conductivity for magnesium oxide can be found in the literature [30] and the diameter of the stainless steel core is estimated (see Table 4.10.).

Table 4.10. The value for the thermal conductivity of magnesium oxide and the estimated diameter of the stainless steel core of the cartridge heater.

Parameter	Value	Unit
k_{MgO}	17.5	W/mK
D_{SS}	0.001	m

Hence, the theoretical value is $(hA)_{CH, \text{theory}} = 7.3$ W/K.

The effect provided from the cartridge heater can be calculated from the maximum effect, which is 2000 W, and the output signal:

$$P = \frac{y}{100} \cdot P_{max} \quad (4.38)$$

where

P Effect of the cartridge heater [W]

y Output signal to the cartridge heater [%]

P_{max} Maximum effect of the cartridge heater [W]

This effect will provide the heat from the heater to the aluminum and in addition, there will be some heat losses to the surrounding.

$$P = Q_{CH} + Q_L \quad (4.39)$$

where

Q_L Heat losses to the surrounding [W]

The heat losses can be described with a heat transfer coefficient and a heat exchange area according to:

$$Q_L = (hA)_L(T_{CH} - T_{amb}) \quad (4.40)$$

where

$(hA)_L$ Heat transfer coefficient and heat exchange area for the losses [W/ K]

T_{amb} Ambient temperature [K]

The heat losses can be calculated with equation 4.39 and the ambient temperature is known to be 20°C. Thereby, the resulting value for the heat transfer is $(hA)_L = 0.48$ W/K.

4.1.3 The Reactor

The reactor is basically a stirred tank with flow of water in and out. Water will be entering the reactor at a lower temperature than the water inside of the reactor. The outlet stream, on the other hand, will have the same temperature as the reactor content. Heating of the reactor is provided through a heating jacket. Figure 4.6 shows a sketch of the reactor with temperatures and heat flow indicated.

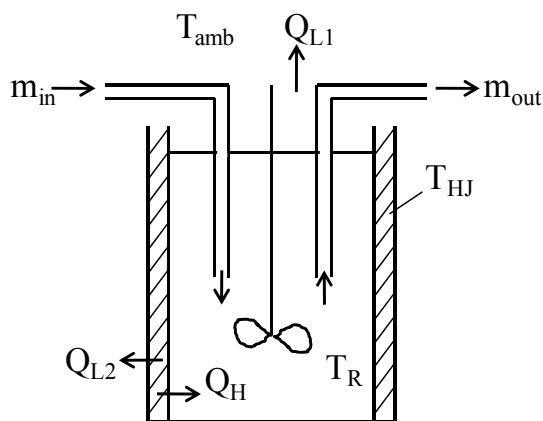


Figure 4.6. Sketch over the reactor. The flows in and out of the reactor are indicated as well as the temperatures and heat flows.

For the reactor modelling, it was assumed that the heating jacket and ambient temperatures were constant. It was also assumed that no energy was transferred from the agitator to the content in the tank due to mixing.

Since the mass flow of water in and out of the reactor is known as well as the temperature of these streams, the amount of energy taken up by the water stream can be calculated according to:

$$Q_w = \dot{m}(H_w^{out} - H_w^{in}) \quad (4.41)$$

where

Q_w Heat taken up by the water stream [W]

\dot{m} Mass flow of water [kg/s]

H_w^{out} Enthalpy of the water out from the reactor [J/kg]

H_w^{in} Enthalpy of the water in to the reactor [J/kg]

The energy input to the heating jacket can also be calculated since the output signal y was measured during the experiments. The output signal is the percentage used of the maximum effect (which is 1250 W) according to:

$$P = \frac{y}{100} \cdot P_{max} \quad (4.42)$$

where

P Effect of the heating jacket [W]

y Output signal [%]

P_{max} Maximum effect of the heating jacket [W]

The effect will provide the energy taken up by the water but there are also some heat losses in the system:

$$P = Q_w + Q_L \quad (4.43)$$

Q_L Total heat losses in the system [W]

These heat losses will be a combination of losses from the top of the tank and losses from the outside of the heating jacket.

$$Q_L = Q_{L1} + Q_{L2} \quad (4.44)$$

where

Q_{L1} Heat losses from the top of the reactor [W]

Q_{L2} Heat losses from the heating jacket [W]

The two contributions to the losses can be calculated separately:

$$Q_{L1} = h_{L1}A_{top}(T_R - T_{amb}) \quad (4.45)$$

$$Q_{L2} = h_{L2}A_{HJ}(T_{HJ} - T_{amb}) \quad (4.46)$$

where

h_{L1} Heat transfer coefficient for the top of the reactor [W/m²K]

A_{top} Heat exchange area at the top of the reactor [m²]

T_R Reactor temperature [K]

T_{amb} Ambient temperature [K]

h_{L2} Heat transfer coefficient for the heating jacket [W/m²K]

A_{HJ} Heat exchange area for the heating jacket [m²]

T_{HJ} Heating jacket temperature [K]

The heat exchange area for the heating jacket is calculated from the circumferences and the heights (see Figure 4.7) according to:

$$A_{HJ} = C_{HJ,1}H_{HJ,1} + C_{HJ,2}H_{HJ,2} \quad (4.47)$$

where

$C_{HJ,j}$ Circumference [m]

$H_{HJ,j}$ Height [m]

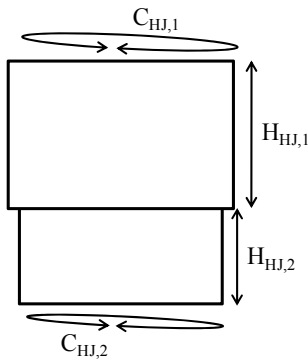


Figure 4.7. The dimensions of the heating jacket.

The heating jacket dimensions and the resulting area can be found in Table 4.11.

Table 4.11. Dimensions and heat exchanger area for the heating jacket.

Parameter	Value	Unit
$C_{HJ,1}$	0.79	m
$H_{HJ,1}$	0.165	m
$C_{HJ,2}$	0.63	m
$H_{HJ,2}$	0.11	m
A_{HJ}	0.20	m ²

The heat exchange area for the top of the reactor can be seen in Figure 4.8 below. A cylinder is located on top of the reactor. The cooling water (cw), which is needed for cooling of the magnetic stirrer, goes through this cylinder. The heat transferred to the cooling water accounts for most of the losses from the top of the reactor. The heat exchange area on the top will be the cross section of the cylinder according to:

$$A_{top} = \frac{\pi D_{top}^2}{4} \quad (4.48)$$

where

D_{top} Diameter of the cylinder on top of the reactor [m]

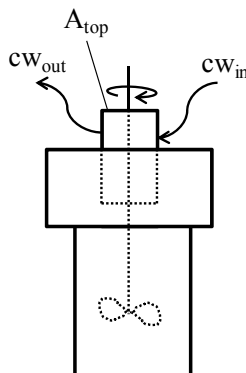


Figure 4.8. Sketch of the reactor. There is a cylinder at the top of the reactor where the cooling water (cw) inlet and outlet for the stirrer are located. The cross section of this cylinder represents the heat exchange area of the top of the reactor.

The value of the diameter can be found in Table 4.12 as well as the heat exchange area at the top.

Table 4.12. The diameter and area of the cylinder situated on top of the reactor.

Parameter	Value	Unit
D_{top}	0.06	m
A_{top}	0.0028	m ²

Since both the heat transfer coefficients in equation 4.45 and 4.46 are unknown, it is not possible to separate the two loss terms from each other. However, the heating jacket, which encloses the reactor, is similar to the one used for heating of the storage tank. This heat

transfer coefficient was calculated for the storage tank. It can be assumed that the heating jacket for the reactor would have a heat transfer coefficient similar to the one for the tank. Therefore, it was set to $h_{L2} = 2 \text{ W/m}^2\text{K}$. This can be compared to conduction through a 4 cm thick insulation material which is about $1 - 2.1 \text{ W/m}^2\text{K}$ ¹⁷ depending on the material.

With the assumed value of h_{L2} , the losses from the heating jacket can be calculated with equation 4.46. Thereby, the heat losses from the top of the reactor will account for the rest of the losses and the heat transfer coefficient h_{L1} can be calculated with equation 4.45. The resulting mean value is $h_{L1} = 195 \text{ W/m}^2\text{K}$. This value can be compared with the value for conduction through 10 cm Inconel 600, which is $190 \text{ W/m}^2\text{K}$ ¹⁸.

The amount of heat lost with the cooling water was examined for one of the experiments, R5. The temperatures in and out were measured as well as the mass flow. The heat taken up by the cooling water can then be calculated with:

$$Q_{cw} = \dot{m}_{cw} C_p \Delta T_{cw} \quad (4.49)$$

where

Q_{cw}	Heat taken up by the cooling water [W]
\dot{m}_{cw}	Mass flow of the cooling water [kg/s]
C_p	Heat capacity of the cooling water [J/kgK]
ΔT_{cw}	Cooling water temperature difference [K]

The resulting values for this experiment can be found in Table 4.13 together with the other calculated heat flows for R5.

Table 4.13. Parameters used for the cooling water calculations.

Parameter	Value	Unit
\dot{m}_{cw}	0.017	kg/s
C_p	4200	J/kgK
ΔT	2	K
Q_{cw}	143	W
Q_L	340	W
Q_{L1}	170	W
Q_{L2}	169	W

The table shows that the heat lost through the top of the reactor, Q_{L1} , is somewhat larger than the amount of heat taken up by the cooling water, Q_{cw} . However, there may be some other losses from the reactor top, e.g. to the surroundings, which can explain this difference. In summary, the model for the heat losses seems to give reasonable results for this case.

¹⁷ The value is calculated from the thermal conductivity $0.04 - 0.085 \text{ W/mK}$ [26].

¹⁸ The value is calculated from the thermal conductivity 19 W/mK [29].

The heat transferred from the heating jacket to the reactor, which will be the sum of the heat taken up by the water in the reactor and the heat losses from the reactor top can now be calculated from:

$$Q_H = Q_w + Q_{L1} \quad (4.50)$$

where

Q_H Heat flow to the reactor from the heating jacket [W]

The heat transfer from the heating jacket to the reactor will consist of transport to the outside of the reactor wall, transport through the wall and transport of heat inside of the reactor.

Since the temperatures are rather high on the outside of the reactor, the heat transfer from the heating jacket to the tank wall can be assumed to be due to radiation:

$$Q_{rad} = \epsilon \sigma A_{HX} (T_{HJ}^4 - T_{wall}^4) \quad (4.51)$$

where

Q_{rad} Radiant heat transfer to the reactor wall [W]

ϵ Emissivity of the reactor wall surface [-]

σ Stefan-Boltzman constant [W/m^2K^4]

A_{HX} Heat exchanger area [m^2]

T_{wall} Temperature of the reactor wall outside [K]

The heat exchange area will be the outside area of the reactor and can be calculated from the diameters and heights (see Figure 4.9) according to:

$$A_{HX} = \pi D_{R,1} H_{R,1} + \pi D_{R,2} H_{R,2} \quad (4.52)$$

where

$D_{R,j}$ Diameter [m]

$H_{R,j}$ Height [m]

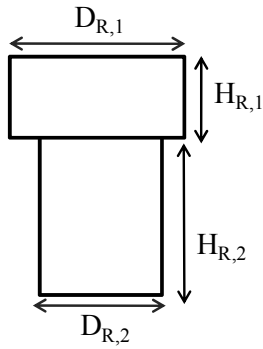


Figure 4.9. The dimensions of the reactor.

The value for the emissivity [28 p. Ka3] and the Stefan-Boltzman constant [27 p. 209] can be found in the literature and can be seen in Table 4.14 together with the dimensions and outside area of the reactor.

Table 4.14. Reactor dimensions and parameters for calculation of radiant heat transfer.

Parameter	Value	Unit
$D_{R,1}$	0.14	m
$H_{R,1}$	0.079	m
$D_{R,2}$	0.095	m
$H_{R,2}$	0.162	m
A_{HX}	0.083	m ²
ϵ	0.69	m ²
σ	5.68E-08	W/m ² K ⁴

The value of Q_H can now be calculated experimentally from equation 4.50 and theoretically from equation 4.51¹⁹. The results show that the theoretical value is somewhat larger than the experimental one. However an emissivity of 0.5 instead of 0.69 would give about the same value for the theoretical case as for the experimental one.

The heat transfer through the reactor wall must equal the amount of heat transported to the wall, if the system is in steady state. It will be due to conduction through the wall material, which is Inconel 600. This conduction can be described with:

$$Q_{wall} = \frac{k_{Inc}}{\delta} A_{HX} (T_{wall} - T_R) \quad (4.53)$$

where

Q_{wall} Heat transfer through the reactor wall [W]

k_{Inc} Thermal conductivity of the reactor wall [W/mK]

δ Reactor wall thickness [m]

¹⁹ The calculations for the reactor heating can be found in Appendix C – Reactor Calculations.

T_R Reactor temperature [K]

The thermal conductivity can be found in the literature [29] and the wall thickness is known. The values of these parameters can be found in Table 4.15:

Table 4.15. Parameters for calculation of heat transport through the reactor wall.

Parameter	Value	Unit
k_{inc}	19	W/mK
δ	0.016	m

The resulting transport of heat through the tank wall was found to be much larger than the heat transported to the reactor which is unreasonable. This is discussed further in Section 5.2.

The heat transport coefficient for the water inside of the reactor was calculated in the same way as in the storage tank case, with equations 4.4 – 4.8. It was found to be very large (8700 – 10400 W/m²K), indicating negligible resistance inside of the reactor. Thereby, the temperature in the reactor can be assumed to be constant.

4.2 Control and Regulation

This chapter contains theory about PID-regulators, which are used for regulation of the pilot plants heating units; heating of the storage tank, the preheater and the reactor. Furthermore, some observations from the experiments are described here.

4.2.1 PID-regulators

The control systems which are studied here concerns the three different heating units mentioned earlier, which are regulated with PID-regulators. A regulated system can be described with a block diagram, which can be seen in Figure 4.10 below.

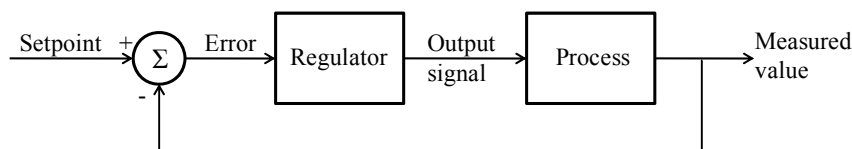


Figure 4.10. Block diagram over a typical regulated system.

The studied heating units can be compared with the block diagram where the setpoint will be the desired temperature of the heater, which is set at the control unit. The output signal will be the effect of the heater, or more correctly, the percentage used of the maximum effect. Moreover, the measured value will be the actual temperature of the heater. Thereby, the error will be the difference between the set and actual value of the heaters temperature.

The regulator will use the error signal to regulate the output signal which is sent to the process, in this case the heater. PID regulators are divided into three parts, with proportional (P), integrating (I) and derivative (D) control [31]²⁰.

Proportional control of the system regulates the output signal by a proportional gain to the error according to:

$$y_P = K \cdot e(t) \quad (4.54)$$

where

y_P Output signal for the proportional controller [-]

K Gain [-]

e Error signal [-]

The output signal will thereby depend on the sign and magnitude of the error signal. A large value of K will result in a faster change in the system, but may also cause instability due to overshoots and oscillations of the output signal. Furthermore, if the measured value is equal to the setpoint value, the output signal will be zero. To compensate for this, an integral term can be added to the proportional term.

The integrating control will take the duration of the error into account, by integrating the error signal over time:

$$y_I = K \cdot \frac{1}{\tau_I} \int_{t_0}^t e(t) dt \quad (4.55)$$

where

y_I Output signal for the integrating controller [-]

τ_I Integration time [s]

A low integration time, T_I , will make the regulator respond quicker to errors. However, low values of T_I will result in an unstable system with low damping of oscillations. Moreover, since the integrating term responds to errors accumulated in the past, it may cause overshoots in the system, which then causes compensation of the error in the other direction and hence increased amplitude of oscillations.

The derivative control predicts the error and uses an expected value to regulate the output signal according to:

$$y_D = K \cdot \tau_D \frac{de(t)}{dt} \quad (4.56)$$

²⁰ This reference was used for this entire section.

where

y_D Output signal for the derivative controller [-]

τ_D Derivative time [s]

Addition of this derivative term will increase the stability in the system, but makes it sensitive to disturbances. A regulator with derivative control may become unstable due to large measurement noise.

In summary, the PID-regulator will calculate the output signal according to:

$$y = K \left(e(t) + \frac{1}{\tau_I} \int_{t_0}^t e(t) dt + \tau_D \frac{de(t)}{dt} \right) \quad (4.57)$$

The values of these PID-parameters were noted for the regulators for the three heating units. They can be found in Table 4.16.

Table 4.16. Regulator parameters for the heaters of the different heated units.

Unit	K [-]	τ_I [s]	τ_D [s]
Storage tank	25.4	62	15
Preheater	31.4	38	9
Reactor	41.6	105	26

4.2.2 Observations from Experiments

The behavior of the regulators was studied during the water experiments. The measured value of the heaters increased rather rapidly after an increase in the setpoint was made. For instance, the heating jacket temperature of the tank increased from 20°C to a setpoint value of 50°C in less than two minutes. The overshoot during this heating period was 2.5°C, but was quickly damped. The cartridge heater inside of the preheater also responded quickly to increases in setpoint temperature. An increase from 20 to 416°C took about six minutes. The same holds for the heating jacket used for heating of the reactor. It took about six minutes to increase the temperature from 20 to 443°C.

The heated units, on the other hand, do not heat up that rapidly. The corresponding time for the tank example mentioned above is about two and a half hour to heat the water inside the tank from 18 to 43°C. Then additional two and a half hour to increase the temperature to the steady state value of 47.5°C. For the preheater, the increase in water outlet temperature was about 245°C in one hour (from 20 to 265°C). The aluminum temperature increased with about the same rate as the water outlet temperature. The temperature increase in the reactor, however, is a bit more complicated to evaluate. Since the water from the preheater enters the reactor, the temperature of the preheater will affect the heating of the reactor. While the water inlet is warmer than the reactor temperature, it will enhance the temperature increase. In the same way, when the water inlet is colder, it will cool down the reactor and reduce the heating rate. However, the increase corresponding to the data in the previous paragraph was 243°C

(from 20 to 263°C) in about one hour (with warmer water inlet than reactor temperature). Then it increased about 60°C more in the following hour (with colder water inlet than the reactor temperature).

It can be concluded that the temperature increase of the heaters is rapid, while the temperature increase of the heated units is rather slow. The reason for this is that the heaters have small masses to heat up, while the heated units have much larger masses.

Furthermore, considering the heated units, the system is rather stable since it responds slowly to changes in temperature. Thereby, it will be easier to regulate since the risk for overshoots and oscillations will be lower. On the other hand, if a change in the output signal gives a slow response in the measured value, there is a chance that the regulator will continue to compensate for the measured error, even if it is about to decrease. This may lead to overcompensation and cause oscillations.

5 Discussion

This chapter contains a discussion of the results from the conducted experiments. The mathematical modeling with its assumptions and simplifications is also evaluated here. Finally, this chapter provides a discussion about the control and regulation of the studied system.

5.1 Experimental Results

The results from the storage tank experiments were quite expected. Higher temperature of the heating jacket gives higher temperature increase in the beginning during heating and a higher final temperature in the tank. Moreover, the heating jacket requires more effect to keep a higher temperature in the tank since more energy is lost to the surroundings. Nevertheless, if rapid heating of the tank to a certain temperature is desired, the heating jacket can be set to a high temperature to start with. This would give a high temperature difference and thereby enhance the temperature increase. Then, when the tank content approaches the desired temperature, the heating jacket temperature can be lowered to a value which gives the desired value at steady state.

It was concluded that the required temperatures of the cartridge heater in the preheater strongly depended on the mass flow of water. That is because more energy is required to increase the water temperature to a certain value if the flow is increased. This is confirmed by the output signal which also increases with the mass flow. Furthermore, higher temperatures are required for higher water outlet temperatures since more heat needs to be transferred to the water stream.

The preheater temperatures were denoted also during the reactor experiments. It was found that a higher temperature of the cartridge heater was needed to obtain a certain temperature of the water outlet during these experiments than when the preheater was evaluated. However, the temperature of the aluminum and the output signal was approximately the same as in the previous trials. This indicates that the heat transfer between the heater and the aluminum has been affected, possibly by some aging phenomena. The value of the constant used to describe the heat transfer will therefore be taken from the reactor experiments.

The reactor experiments showed that high reactor temperature, cold inlet water stream and high mass flow requires higher temperatures on the heating jacket and the outside of the reactor wall. The higher temperatures correspond to larger heat transfer to the reactor, which gives a higher temperature on the inside. Furthermore, since the entering water has a lower temperature than the water inside of the reactor, it provides cooling of the reactor. Thereby, lower temperatures of the water inlet and higher mass flows increases the cooling of the system. A large amount of cooling will of course require a large amount of heating. In addition, there is a larger temperature difference between the heating jacket and the reactor wall than between the outside of the reactor wall and the inside of the reactor. This implies

that there is a higher heat transfer resistance from the heating jacket to the wall than through the wall.

The pump trials with lignin slurry at different concentrations showed that it is possible to pump slurries at low concentrations (5 and 10 wt% lignin). However, when more concentrated slurries are used, the pump will struggle to recirculate it back to the tank. The highest concentration (40 wt% lignin) was not possible to pump at all. The limiting factor is probably the two non-return check valves at the inlet and outlet of the pump since it started to work again after cleaning of the valves.

5.2 Mathematical Modelling

In the modelling of the storage tank, the radiant heat transfer was neglected even though it accounted for up to 20% of the total heat transfer. However, the heat transfer coefficient, h_{tot} , was calculated to represent the total heat transfer. In that way, the radiant heat transfer contribution will be included anyway.

During the calculations of heat transfer area for the preheater, the dimensions were estimated from pictures and measurements of the installed equipment. These estimations are of course not ideal for calculations of the heat exchanger areas. Nevertheless, since there was no other alternative, they were assumed to be accurate enough to give a reasonable model of the preheater.

The overall heat transfer coefficient from aluminum to water was calculated both from the experimental results and theoretically. The theoretical value was calculated for laminar flow in a pipe. Due to the low ratio between the inside diameter of the pipe and the pipe length, the Nusselt number was close to 3.65 and the calculated heat transfer coefficient about the same for all cases. It was also found that the theoretically calculated value of the overall heat transfer coefficient was much higher than the experimentally determined one. Many possible reasons for this were considered²¹.

One possible explanation could be that most of the heat is transferred at the highest temperature difference, i.e. where the water enters the preheater. The water would then be heated in the first section of the preheater, while it is just kept at a constant temperature through in the rest of the pipe distance. The resulting temperature profile is shown in Figure 5.1. The effective area of heat exchange would then be less than the one used here since some of it remains unused. This was investigated by calculating the experimental U-value for a heat exchange area of only 10% of the original one. The resulting values of the overall heat exchange coefficient still differed from the theoretical one with more than 100 W/m²K for the lowest flow rate. Hence, unused heat exchange area is not a sufficient explanation for the low experimental U-values.

²¹ The calculations for these investigations can be found in Appendix B – Preheater Calculations.

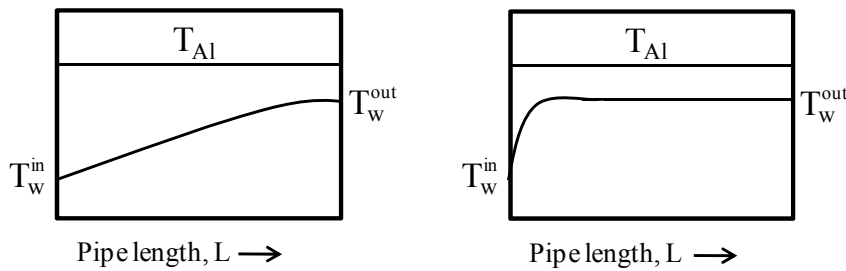


Figure 5.1. Temperature profiles. The picture to the left shows a temperature profile where the entire heat exchange area is used. The temperature increases throughout the pipe length. The right picture shows a temperature profile over a heat exchanger with an unused heat exchange area. The temperature increases a lot in the first part of the pipe, while it is kept constant through the rest of the pipe length.

Another possibility is that the water outlet is cooled down by the box in which the preheater is situated. In that way, the water outlet temperature, which is measured in the pipe some distance after the preheater, will be lower than the actual temperature at the preheater outlet. This would mean that the temperature increase is underestimated in the calculations, resulting in an underestimation of the experimental U-value. However, it was found that the temperature decrease due to this cooling would have to be large in order to explain the deviation from the theoretical U-value and that is not realistic.

The measured aluminum temperature could be misleading due to a temperature gradient in the aluminum. That would mean that the assumption that this temperature is constant throughout the body would be wrong. This was investigated by assuming an U-value of $460 \text{ W/m}^2\text{K}$ for the experimental calculations and calculating the corresponding logarithmic mean temperature. The resulting aluminum temperature could then be found. Though, the temperature difference between the aluminum and the water outlet would have to be much less than 1°C for this assumption to hold, which is completely unrealistic.

There could also be some other resistance that affects the heat transfer. One possibility is that there is a small passage of air. This could have been created around the water pipe when the preheater was manufactured. A small passage of 0.36 mm would be enough to decrease the U_{theory} to a value of $100 \text{ W/m}^2\text{K}$, which is the same as for the highest flow rate.

In summary, the most likely of these investigated reasons for the difference between the theoretical and experimental U-value is that there is a small passage of air which reduces the theoretical U-value. However, it was also found that the experimental U-value increased with the mass flow of water. This cannot be explained with convection through a passage of air. On the other hand, if the heat transport through this air passage was modeled as radiant heat transfer, it would not be proportional to the temperature. Radiant heat transfer increases more with temperature than heat transfer due to convection and conduction. Thus, a small increase in temperature would give a larger increase in heat transfer. The theoretical U-value would thereby be larger for higher temperatures of the aluminum, which were required for higher mass flows. This could be one explanation for the variation in U-value with the mass flow of water.

Furthermore, there could also be some other phenomena which influence the heat transfer in the preheater. For instance, the flow through the pipe is modeled as laminar flow through a straight pipe. Though, the fact that the water pipe is wired like a coil has not been taken into account. For instance, gravitational and centrifugal forces are not considered. This could influence the flow in the pipe and probably increase the Reynolds number. These effects could also be related to the mass flow of water. On the other hand, higher Reynolds number would enhance the heat transfer and make the theoretical U-value higher. The difference between the theoretical and experimental values would thereby be even larger. It is impossible to tell what the actual reason for the difference in heat transfer coefficient value is without a more thorough examination of the preheater. Other phenomena than those discussed here could influence the heat transfer as well and it could be a combination of different phenomena.

During the modelling of the reactor, it was assumed that the heat transfer coefficient of the heating jacket would be about the same as for the tank's heating jacket. The two heating jackets seem to be constructed in a similar way, with similar material. Thereby, the heat transfer coefficient should be about the same as well. It was necessary to estimate this coefficient in order to separate the two loss terms from each other. The assumption was validated by calculation of the amount of heat lost with the cooling water at the top of the reactor. The cooling water was found to account for most of the losses from the top. In addition, there will probably be some losses to the surroundings as well.

Furthermore, the radiant heat transfer was calculated. It was found to be higher than the total heat transferred from the heating jacket to the reactor. However, the value of the emissivity, taken from the literature [28 p. Ka 3], corresponds to a temperature of 816°C ²². The emissivity depends on the temperature and the reactor wall is below 400°C at all times. Thereby, the true value of the emissivity may be lower in reality. It was found that an emissivity of 0.5 would give the same value of the radiant heat transfer as for the total heat transfer to the reactor.

The heat transport through the reactor wall was also calculated. However, it was found to be much larger than the total heat transfer to the reactor. This is of course not realistic. One explanation could be that the measured value of the temperature on the outside of the reactor wall is inaccurate and thereby misleading. The influence of the thermal conductivity value was investigated. It needs to be as low as 3.5 W/mK for the heat transport through the wall to equal the total heat transfer. This can be compared with 19 W/mK which is found in the literature [29] for a temperature about 300°C .

5.3 Accuracy of Measurements

The effect of inaccuracy in measured values from the experiments has been examined. For the modelling of the tank, the largest insecurity lies within the measured value of the output signal. The output signal is given in percentages, where each percent corresponds to an effect

²² Recalculated from Kelvin.

of 20 W. However, the error margin of this measured value is $\pm 0.5\%$, this means that the value 1% could correspond to 0.5 – 1.5 % which gives the effects 10 – 30 W. This insecurity in the output signal will affect the accuracy of the calculated value of the heat transfer coefficient for the losses from the tank's heating jacket. Inaccuracies in temperature measurements on the other hand, will not affect this calculated value as much.

During the preheater experiments, the temperature of the water in the tank varied within an interval of about 10°C , but this did not influence the performance of the preheater at all. The water properties used for calculation of the theoretical U-value were taken as mean values for the temperature intervals. It was previously mentioned that the low ratio of the diameter and pipe length gives a Nusselt number close to 3.65 for all examined water conditions. Thus, the heat transfer coefficient will only be affected by the used value of the water's thermal conductivity, which varied between 0.55 – 0.70 W/mK within the temperature interval 40 – 310°C . The heat transfer coefficient for the water in the pipe will thereby vary between 530 – 660 W/m²K, which gives a variation in theoretical U-value between 420 – 500 W/m²K. The heat transfer resistances in the aluminum and the water pipe will not affect this theoretical U-value as much, since they are a lot smaller than the resistance in the water. The output signal for the preheater has the same error margin for the measured value as the tank. Though, this did not influence the heat losses from the cartridge heater that much. The value for the heat transfer coefficient and area for these losses only varies with ± 0.05 W/K for a change in output signal with $\pm 1\%$.

The heat transfer coefficient for the losses from the top of the reactor depends on the chosen value of the coefficient for the losses from the outside of the heating jacket. A change in this chosen value with ± 0.2 W/m²K gives a change of ± 20 W/m²K for the losses from the top of the reactor. Variations in output signal to the heating jacket, i.e. the effect, does not influence the heat transfer coefficient for the top as much.

The output signal affects the results for the tank more than the results for the preheater and the reactor. That is probably since for the tank, the signal is only a few percent, while the signal for the preheater and the reactor is more than 20 % in all cases. The difference between 0.5 – 1.5 % will affect the results more than the difference between 19.5 – 20.5 %.

5.4 Control and Regulation

The observations of the system during the water experiments showed that the heaters respond quickly to changes in temperature. The heated units, on the other hand, react slowly to changes in temperature of the heater. The heated units have much larger masses, resulting in longer heat up times.

Since the heated units are less sensitive to changes in temperature, the system will be more stable and probably easier to regulate. A large change in output signal is less likely to cause overshoots since the system responds slowly. On the other hand, slow changes in the system may cause oscillations due to overcompensations from the regulator.

The temperature increase of the heated units will also depend on the temperature difference between the heater's temperature and the temperature of the heated unit. A large difference will give a large driving force and a quicker increase in temperature. Since it is the temperature of the heater that is regulated this will not be taken into account. However, it can be controlled manually by setting a higher temperature than needed on the heater. Then, when the heated unit approaches the desired temperature, the heater can be set to a lower value. Another option is to regulate the temperature of the heated unit instead of the heater. Thereby, the time for heating will probably be reduced. On the other hand, the temperature limits of the different parts of the plant must be taken into consideration.

The experiments have shown that temperatures of up to 350°C in the reactor is possible to obtain without exceeding any of the temperature limits. The reactor wall temperature was about 390°C in the most demanding case. Hence, far from the temperature limit of 500°C. However, a colder inlet stream to the reactor will require a higher temperature on the heating jacket and the reactor wall. The desired temperatures in the preheater and storage tank could also be obtained without exceeding any temperature limits.

6 Conclusions

Mathematical models have been set up for the heated units of the pilot scale plant; the storage tank, the preheater and the reactor. The resulting equations can be seen below.

The heating of the storage tank and the heat from the heating jacket can be described by:

$$\rho V C_p \frac{dT_w}{dt} = h_{tot} A_{HX} (T_{HJ} - T_w) - h_{L1} A_{cs} (T_w - T_{amb}) \quad (6.1)$$

$$P = h_{tot} A_{HX} (T_{HJ} - T_w) + h_{L2} A_{HJ} (T_{HJ} - T_{amb}) \quad (6.2)$$

The heat transfer coefficients and areas can be found in Section 4.1.1. The value of the density and heat capacity will depend on the water temperature in the tank. It will also change if another medium is used.

The heat transfer to the water passing through the preheater and the heat from the cartridge heater to the aluminum can be described by:

$$Q_{HX} = U A_{HX} \Delta T_{lm} \quad (6.3)$$

$$P = (hA)_{CH} (T_{CH} - T_{Al}) + (hA)_L (T_{CH} - T_{amb}) \quad (6.4)$$

The heat transfer coefficients and areas can be found in Section 4.1.2. The value of the overall heat transfer coefficient was found to vary with the flow of water in the pipe (see Table 4.8). It will also change if another medium is used.

The heat from the reactor heating jacket and the heat taken up by the water stream that goes through the reactor can be described with:

$$P = \sigma \epsilon A_{HX} (T_{HJ}^4 - T_{wall}^4) + h_{L2} A_{HJ} (T_{HJ} - T_{amb}) \quad (6.5)$$

$$\dot{m} C_p (T_R - T_w^{in}) = \sigma \epsilon A_{HX} (T_{HJ}^4 - T_{wall}^4) - h_{L1} A_{top} (T_R - T_{amb}) \quad (6.6)$$

The heat transfer coefficients and areas can be found in Section 5.4 as well as the value for the emissivity and Stefan-Boltzman constant. The value of the heat capacity will depend on the water temperature in the tank. It will also change if another medium is used.

Moreover, the pump trials showed that lignin slurries of higher concentrations than 10 wt% lignin could not be pumped easily with the existing pump.

During the water experiments, it could be seen that the heaters can supply enough heat to reach water temperatures up to 350°C inside of the reactor. They should thereby be sufficient to use for the purpose of providing heat up to the supercritical point of water.

7 Further Research

The aim of this master's thesis work was to evaluate the pilot scale plant, which afterwards will be used in further research. Mathematical models have been presented which describes the heat transfer in the storage tank, the preheater and the reactor. However, the thesis work is only a first step in a larger project which aims to find a method for converting lignin or black liquor into liquid fuels. There is still a lot of work to be done within this project.

Simulations of the heat transfer in different parts of the plant could be done in order to improve the heating models further. In that way, the difference between the theoretical and experimental U-value of the preheater may be explained.

It could also be examined if it is possible to regulate the temperature of the heated units instead of the heaters. Thereby, it would be easier to obtain the desired temperatures in the different parts of the plant. Though, such a regulation will be more complicated and a thorough investigation is needed since it is important that the temperature limits are not exceeded.

The pump trials with lignin showed that the pump could only operate with slurries of low lignin concentration. Some addition to the slurry could be investigated aiming to obtain a mixture which can be pumped at higher lignin concentrations. Other types of feedstock could also be tested in the plant. The optimum operating temperature and pressure should be investigated as well as residence time.

In addition, a catalyst will be introduced to the system. One task is to decide which kind of catalyst and then perform experiments. It is important to achieve optimum reaction rate. The reaction will have to be fast enough for sufficient amount of material to react. On the other hand, a too fast reaction may result in a gasification of the material and the aim is to find a liquid fuel.

The reactor plant may also be partially extended and/or rebuilt. For instance, there are plans to add one more pump to the system. In that way, two fluids can be pumped separately to the reactor and be mixed at the inlet.

The project, aiming to find a method for conversion of lignin and/or black liquor to liquid fuels has only been initiated. It will probably continue for a few years and many other ideas will be evaluated.

References

1. **Harvey, Simon.** CO2 Emissions From Industrial Energy Systems. *Course Compendium in Industrial Energy Systems*. Göteborg : Chalmers University of Technology, 2008.
2. **Sircharoenchaikul, V.** Assessment of black liquor gasification in supercritical water. *Bioresource Technology*. 100, 2009, 638-643.
3. **Råberg, Mathias.** *Black liquor gasification - Experimental stability studies of smelt components and refractory lining*. Umeå : Energy Technology and Thermal Process Chemistry, Umeå University, 2007. ISBN 978-91-7264-339-0.
4. **Eriksson, H and Harvey, S.** Black liquor gasification - consequences for both industry and society. *Energy*. 29, 2004, 581-612.
5. *Pilot-scale combustion studies with kraft lignin as a solid biofuel.* **Berglin, N, et al.** Portland, Oregon : Pulping and Environmental Conference, August 25-27, 2008.
6. **Brodin, Ida, Sjöholm, Elisabeth and Gellerstedt, Göran.** Kraft lignin as feedstock for chemical products: The effects of membrane filtration. *Holzforschun*. 2009, Vol. 63, 290-297.
7. **Sweden Energy Agency.** *Energy in Sweden 2009*. 2009.
8. *The LignoBoost process.* **Tomani, Per.** Helsinki, Finland : NWBC, September 2-4, 2009.
9. **Resende, Fernando L. P, et al.** Noncatalytic Gasification of Lignin in Supercritical Water. *Energy & Fuel*. 22, 2008, 1328-1334.
10. **Kleinert, Mike and Barth, Tanja.** Towards a Lignin-cellulosic Biorefinery: Direct One-Step Conversion of Lignin to Hydrogen-Enriched Biofuel. *Energy & Fuels*. 2008, Vol. 22, 1371-1379.
11. **Barth, Tanja and Kleinert, Mike.** Motor Fuels From Biomass Pyrolysis. *Chemical Engineering & Technology*. 31, No. 5, 2008, 773-781.
12. **Huibers, Derk T. A and Parkhurst, Hugh J. Jr.** *Lignin Hydrocracking Process to Produce Phenol and Benzene*. 4 420 644 United States Patent, December 13, 1983.
13. **Engel, Dusan J and Steigleder, Karl Z.** *Hydrocracking Process for Liquefaction of Lignin*. 4 647 704 United States Patent, Mars 3, 1987.
14. **Sricharoenchaikul, Viboon, Frederick Jr, Wm. James and Agrawal, Pradeep.** Carbon distribution in char residue from gasification of kraft black liquor. *Biomass and Bioenergy*. 25, 2003, 209-220.
15. **Timpe, Winfred G.** *Pyrolysis of Spent Pulping Liquors*. 3 762 989 United States Patent, October 2, 1973.

16. **Gilbert, Allan F and Cooper, Dave F.** Hydropyrolysis of Kraft Hardwood and Softwood Black Liquor. *The Canadian Journal of Chemical Engineering*. 1987, Vol. 65.
17. **Producing Oil From Black Liquor. Creasy, Dennis and Covey, Geoff.** Appita Conference : s.n., 2003.
http://www.coveyconsulting.com.au/Documents/paper_gc_dc_producing_oil_from_black_liquor.pdf.
18. **Elliott, Douglas C and Oasmaa, Anja.** Catalytic Hydrotreating of Black Liquor Oils. *Energy & Fuels*. 5, 1991, 102-109.
19. **Shaw, R W, et al.** Supercritical water - A Medium for Chemistry. *Chemical Engineering News*. 1991, December 23, 26.
20. **Bröll, Dirk, et al.** Chemistry in Supercritical Water. *Angewandte Chemie International Edition*. 38, 1999, 2998-3041.
21. **Savage, Phillip E.** A perspective on catalysis in sub- and supercritical water. *Journal of Supercritical Fluids*. 47, 2009, 407-414.
22. **Brunner, G.** Near critical and supercritical water. Part I. Hydrolytic and hydrothermal processes. *Journal of Supercritical Fluids*. 47, 2009, 373-381.
23. **Kruse, A and Dinjus, E.** Hot compressed water as reaction medium and reactant properties and synthesis reactions. *Journal of Supercritical Fluids*. 39, 2007, 362-380.
24. **Sigmar Mothes Hochdrucktechnik GmbH.** *Autoklavenstation - Plant Description and Operating Instructions*. Berlin : s.n., 2009.
25. **Sinnott, Ray and Towler, Gavin.** *Chemical Engineering Design*. s.l. : Butterworth-Heinemann, imprint of Elsevier, 2009. ISBN: 978-0-7506-8551-1.
26. **Mörtstedt, Sven-Erik and Hellsten, Gunnar.** *Data och Diagram*. Malmö : Liber AB, 2003. ISBN 91-47-00805-9.
27. **Welty, James R, et al.** *Fundamentals of Momentum, Heat and Mass Transfer (Appendix H)*. s.l. : John Wiley & Sons Inc., 2001. ISBN 0-471-38149-7.
28. **Verein Deutscher Ingenieure.** *VDI - Wärmeatlas*. Düsseldorf : VDI-Verlage, 1988.
29. **High Temp Metals inc.** [Online] [Cited: 04 13, 2010.]
<http://www.hightempmetals.com/techdata/hitempInconel600data.php>.
30. **Slifka, A J, Filla, B J and Phelps, J M.** Thermal Conductivity of Magnesium Oxide From Absolute, Steady-State Measurements. *Journal of Research of the National Institute of Standards and Technology*. 4, 1998, Vol. 103.
31. **Glad, Torkel and Ljung, Lennart.** *Reglerteknik - Grundläggande teori*. Lund : Studentlitteratur, 1995. ISBN 91-44-17892-1.

32. **National Institute of Standards and Technology.** NIST Chemistry WebBook. [Online] 2008. [Cited: 05 04, 2010.] <http://webbook.nist.gov/chemistry/>.

33. **Grenoble, D C, Estadt, M M and Ollis, D F.** The Chemistry and Catalysis of the Water Gas Shift Reaction. *Journal of Catalysis.* 67, 1981, 90-102.

Appendix A – Storage Tank Calculations

Heat Transfer Coefficient for the Water in the Tank

Table A. 1. Data and resulting values for the calculation of the heat transfer coefficient for the water in the tank. The constants C , a and b are found in the literature [25 p. 959].

C [—]	a [—]	b [—]	Re [—]	Pr [—]	Nu [—]	h_w [W/m ² K]
0.54	0.67	0.33	42683	3.2	1005	6531
0.74	0.67	0.33	42683	3.2	1377	8950
1.1	0.62	0.33	42683	3.2	1201	7807

$$Re = \frac{ND^2\rho}{\mu}$$

$$Pr = \frac{\mu C_p}{k_w}$$

$$Nu = C \cdot Re^a \cdot Pr^b$$

$$h_w = \frac{NuD}{k_w}$$

Table A. 2. Constants used for the calculation of the heat transfer coefficient for the water in the tank. The properties of the water are found in the literature [26]. Mean values between 20 and 75°C at atmospheric pressure has been used.

ρ	985	kg/m ³
μ	0.0005	Pas
C_p	4181	J/kgK
k_w	0.65	W/mK
D	0.1	m
N	2.17	rps

Appendix B – Preheater Calculations

Calculations of the Water Heat Transfer Coefficient

Table A. 3. Data and resulting values for the water heat transfer coefficient. The values for the water properties are found in the literature [32]. Mean values between 40°C and the water outlet temperature has been used at 200 bar. The mean value for the water heat transfer coefficient can be found below the table.

Test	μ [Pas]	C_p [J/kgK]	k_w [W/mK]	Re [—]	Pr [—]	Nu [—]	h_w [W/m ² K]
PH3	0.00019	4238	0.64	455.37	1.2858	3.733	597
PH6	0.00019	4238	0.64	910.74	1.2858	3.791	607
PH9	0.00019	4238	0.64	1366.11	1.2858	3.841	615
PH12	0.00018	4272	0.62	505.20	1.2058	3.736	579
PH15	0.00018	4272	0.62	1010.39	1.2058	3.795	588
PH18	0.00018	4272	0.62	1515.59	1.2058	3.847	596
PH21	0.00015	4312	0.61	574.39	1.0882	3.738	570
PH24	0.00015	4312	0.61	1148.79	1.0882	3.798	579
PH27	0.00015	4312	0.61	1723.2	1.0882	3.851	587
PH28	0.00019	4238	0.64	1138.43	1.2858	3.817	611
PH29	0.00018	4272	0.62	1262.99	1.2058	3.822	592
PH30	0.00015	4312	0.61	1435.99	1.0882	3.825	583

592

$$Re = \frac{4\dot{m}}{\mu\pi D_i}$$

$$Pr = \frac{\mu C_p}{k_w}$$

$$Nu = 3.65 + \frac{0.19(Re \cdot Pr \frac{D_i}{L})^{0.8}}{1 + 0.117(Re \cdot Pr \frac{D_i}{L})^{0.467}}$$

$$h_w = \frac{k_w Nu}{D_i}$$

Table A. 4. Constants used for the calculation of the water heat transfer coefficient.

D_i	0.004	m
L	6	m

The value of Nu will be close to 3.65 since the term $\frac{D_i}{L}$ will be very small. Therefore, the heat transfer coefficient will be about the same for all experiments.

Calculations for the Preheater Discussion

The calculations for the discussion of the preheater modelling discussed in Section 5.2. can be found below.

Table A. 5. Data and resulting values for the cartridge heater heat transfer from the preheater experiments.

Test	U [W/m ² K]	ΔT_{lm} [K]	U [W/m ² K]	$\Delta T_{lm,1}$ [K]	$\Delta T_{lm,2}$ [K]
PH3	354.4	114.9	288.9	7.2	53.8
PH6	708.8	114.9	577.9	14.4	53.8
PH9	1000.8	119.9	831.0	21.7	53.8
PH12	357.8	129.2	298.4	8.4	58.0
PH15	715.5	129.2	596.8	16.8	58.0
PH18	993.3	136.7	846.0	25.1	58.0
PH21	368.6	142.1	312.0	9.6	62.1
PH24	737.2	142.1	624.0	19.3	62.1
PH27	998.2	153.5	866.6	28.9	62.1
PH28	872.2	116.2	714.6	18.1	53.8
PH29	848.5	134.2	718.0	21.0	58.0
PH30	859.0	149.7	740.3	24.1	62.1

1
2
3

1: The possibility of unused heat exchange area was evaluated by calculating the overall heat transfer coefficient for 10% of the actual area.

$$U = \frac{Q_w}{0.1 \cdot A_{HX} \Delta T_{lm}}$$

2: The logarithmic mean temperature and resulting overall heat transfer coefficient were calculated for a temperature 20°C higher than the measured one. This was done to investigate if the difference in theoretical and experimental U-value could be due to cooling of the water outlet.

$$\Delta T'_2 = \Delta T_2 + 20$$

$$\Delta T_{lm} = \frac{\Delta T_1 - \Delta T'_2}{\ln\left(\frac{\Delta T_1}{\Delta T'_2}\right)}$$

$$U = \frac{Q_w}{A_{HX} \Delta T_{lm}}$$

3: The possibility of a temperature gradient in the aluminum was investigated by assuming an U-value of 460 W/m²K and calculating the corresponding logarithmic mean temperature. The resulting value, $\Delta T_{lm,1}$, was very low which implies a low aluminum temperature. This value was then compared to a logarithmic mean temperature where the aluminum temperature is assumed to be only 1°C higher than the water outlet temperature, $\Delta T_{lm,2}$. This second mean temperature was a lot higher than the first one, which means that the temperature difference

between the aluminum and the water outlet must be much less than 1°C to give the calculated values of $\Delta T_{lm,1}$.

$$\Delta T_{lm,1} = \frac{Q_w}{460 \cdot A_{HX}}$$

$$T'_{Al} = T_w^{out} + 1$$

$$\Delta T'_1 = T'_{Al} - T_w^{in}$$

$$\Delta T'_2 = 1$$

$$\Delta T_{lm,2} = \frac{\Delta T'_1 - \Delta T'_2}{\ln\left(\frac{T'_1}{\Delta T'_2}\right)}$$

4: The thickness of the air passage required to give a U-value of 100 W/m²K was calculated according to:

$$\sum R = \frac{1}{U} = \frac{1}{100} = 0.01 \text{ m}^2\text{K/W}$$

$$R_{air} = \sum R - R_{Al} - R_{Inc} - R_w = 0.01 - 0.0016 - 0.000056 - 0.00042 = 0.0078 \text{ m}^2\text{K/W}$$

$$R_{air} = \frac{\delta_{air}}{k_{air}}$$

$$\delta_{air} = R_{air} \cdot k_{air} = 0.0078 \cdot 0.0454 = 0.00036 \text{ m}$$

The value of the thermal conductivity of air was found in the literature [26].

Table A. 6. Constants used for the calculation of the cartridge heater heat transfer.

T_w, in	40	°C
A_{HX}	0.075	m ²

Appendix C – Reactor Calculations

Calculations of the Reactor Heating

Table A. 7. Data and resulting values for the reactor heating. The mean value for the emissivity can be found below the table with the calculated values.

Test	Q _H [W]	Q _{wall} [W]	Q _{rad} [W]	ε' [-]
R1	250.0	1391.9	324.8	0.53
R2	358.6	2087.8	503.4	0.49
R3	492.6	2883.2	707.8	0.48
R4	215.7	1292.5	292.7	0.51
R5	305.7	1988.4	385.4	0.55
R6	394.9	2485.5	506.9	0.54
R7	298.5	1590.7	407.2	0.51
R8	483.6	2584.9	677.4	0.49
R9	689.4	3877.4	964.6	0.49
R10	288.0	1491.3	385.0	0.52
R11	423.2	2485.5	552.5	0.53
R12	581.5	3330.6	789.5	0.51

0.51

$$H_{top} = \frac{k_{inc}}{h_{L1}}$$

$$Q_{wall} = \frac{k_{inc}}{\delta} A_{HX} (T_{wall} - T_R)$$

$$Q_{rad} = \epsilon \sigma A_{HX} \left((T_{HJ} + 273)^4 - (T_{wall} + 273)^4 \right)$$

$$\epsilon' = \frac{Q_H}{\sigma A_{HX} \left((T_{HJ} + 273)^4 - (T_{wall} + 273)^4 \right)}$$

Table A. 8. Constants used for the reactor heating. The thermal conductivity [29], emissivity [28 p. Ka3] and Stefan-Boltzman coefficient [27 p. 209] are found in the literature.

k _{inc}	19	W/mK
δ	0.016	m
A _{HX}	0.083	m ²
ε	0.69	–
σ	5.676E-08	W/m ² K ⁴